High bacillary burden and the ESX-1 type VII secretion system promote MHC class I presentation to CD8 T-cells during *Mycobacterium tuberculosis* infection

Author List:

Daniel Mott[1,2], Evelyn Chang[1,2], Tomoyo Shinkawa[2], Jason Yang[1,2], Christina Baer[2], Kadamba Papavinasasundaram[2], Christopher M. Sassetti[1,2], and Samuel M. Behar[1,2,*]

Author Affiliations:

1. Immunology and Microbiology Program, Graduate School of Biomedical Science, University of Massachusetts Medical School, Worcester, Massachusetts, USA.
2. Department of Microbiology and Physiological Systems, University of Massachusetts Medical School, Worcester, Massachusetts, USA.

*Correspondence:

Samuel M. Behar

E-mail address: samuel.behar@umassmed.edu (SMB)

Abstract (150)

Mycobacterium tuberculosis (Mtb) subverts host defenses to persist in macrophages despite immune pressure. CD4 T-cells can recognize macrophages infected with a single bacillus *in vitro*. Under identical conditions, CD8 T-cells inefficiently recognize infected macrophages and fail to restrict Mtb growth, although they can inhibit Mtb growth during high burden intracellular infection. We show that high intracellular Mtb numbers cause macrophage death, leading other macrophages to scavenge cellular debris and cross-present TB10.4 antigen to CD8 T-cells. Cross-presentation by heavily infected macrophages requires the ESX-1 type VII secretion system, indicating that phagosomal membrane damage and cell death promote class I MHC cross-presentation during Mtb infection. Single cell RNAseq shows TB10.4-specific CD8 T-cells are activated and resist T-cell exhaustion, particularly late during infection. Differences in the activation state between TB10.4-specific and other clonally expanded CD8 T-cells supports the idea that different microbial antigens can drive both beneficial and detrimental types of T-cell responses.

Introduction

Despite concerted efforts to eradicate tuberculosis (TB), it persists as one the deadliest infectious diseases globally[1]. First tested in 1921, Bacillus Calmette–Guérin (BCG) remains the only approved vaccine against *Mycobacterium tuberculosis* (Mtb), and yet its efficacy is variable among human populations and it fares poorly at preventing pulmonary tuberculosis[2,3]. With an increased incidence of TB caused by multi-drug resistant strains, the push for a more effective vaccine is urgent, and a better understanding of protective immunity is vital[1].

Impaired cellular immunity caused by conditions as diverse as malnutrition and HIV infection are risk factors for progression to active TB, which highlight the importance of T-cells in containing Mtb infection[4–6]. As in humans, T-cell responses are essential for control of Mtb infection in mice[7,8]. Although CD4 T-cells appear to contribute more to protection than CD8 T-cells in mice, optimal protection is achieved only when both T-cell subsets are present[9,10]. Mtb's success as a pathogen is attributed to its immune evasion strategies, including manipulation of vesicular trafficking and exploitation of immune responses to generate favorable environments for bacterial growth, dissemination, and transmission[11,12]. To develop more effective vaccines, it is crucial that we understand what a successful immune response entails.

Viral and intracellular microbes such as influenza and *Listeria monocytogenes* assemble or replicate in the cytosol of infected cells. There, their antigens are sampled by class I MHC (hereafter, MHC I) and presented to CD8 T-cells, which play a key role in protection against these pathogens[13,14]. Canonical MHC I presentation samples cytosolic antigens, which are processed by the proteasome and loaded onto MHC I in the endoplasmic reticulum (ER)[15]. For extracellular antigen sources, such as extracellular bacteria or tumor cells, antigen presenting cells (APC) engulf the pathogen or apoptotic tumor cell by phagocytosis or efferocytosis, respectively, and use cross-presentation (XPT) to shuttle antigens from endosomal compartments into the MHC I presentation pathway[16]. These pathways are also crucial for the presentation of intracellular pathogens that reside in endosomal compartments. Two different

XPT pathways have been defined. The cytosolic pathway transports antigens out of endosomes or phagosomes and into the cytosol where they are sampled by the canonical MHC I pathway[15,17,18] . In the vacuolar pathway, antigen processing and MHC I loading occur within endosomal compartments, bypassing the canonical MHC I pathway[19–21]. The selection of the XPT pathway depends on the nature of the antigen and the APC phenotype[19–22]. While XPT is associated with DC priming of T-cells, macrophages also cross-present antigens to CD8 T-cells [23]. Since most Mtb-infected cells are macrophages[24], we are interested in how macrophage XPT RENS or non-RENS (expanded or non-expanded) affects CD8 T-cell mediated protection against TB.

Mice mount a substantial CD8 T-cell response following Mtb infection. In infected C57BL/6 (B6) mice, up to 40% of CD8 T-cells in the lung recognize the TB10.4$_{4\text{-}11}$ epitope, making TB10.4 the most immunodominant antigen in this model[25]. To determine the potential of vaccine-elicited CD8 T-cells to mediate protection against Mtb infection, we elicited memory TB10.4$_{4\text{-}11}$-specific CD8 T-cells using a peptide-based vaccine; however, TB10.4$_{4\text{-}11}$-specific CD8 T-cells failed to enhance control of Mtb challenge[26]. In parallel, we generated TB10.4$_{4\text{-}11}$-specific CD8 T-cell lines, which express TCRs of different affinities (e.g., RG3 and RG4)[27]. The RG3 and RG4 CD8 T-cell lines are activated when they recognize their cognate antigen either in the form of γ-irradiated Mtb or synthetic peptide, but they fail to recognize lung myeloid cells isolated from Mtb-infected mice, or *in vitro* infected BMDM or thioglycolate-elicited peritoneal macrophages (TGPM)[28,29]. Under identical conditions and in stark contrast, CD4 T-cell lines specific for the Mtb antigens Ag85B or ESAT6 recognize Mtb-infected macrophages and inhibit intracellular Mtb growth[26,29].

We suggest that the inability of vaccine-elicited TB10.4-specific CD8 T-cells to protect mice against Mtb arises from their inability to recognize Mtb-infected macrophages. The poor recognition of infected macrophages could explain why CD8 T-cells have only a modest impact on control of Mtb infection. The discrepancy between the immunodominance of TB10.4-specific

CD8 T-cells and their inability to recognize Mtb-infected macrophages, is paradoxical and has led us to hypothesize that TB10.4 is a decoy antigen[28,29]. These data motivated us to determine under what conditions Mtb antigens are cross-presented by macrophages and recognized by CD8 T-cells.

Results

Infected macrophages poorly activate Mtb-specific CD8 T-cells

To determine whether the inability of CD8 T-cells to recognize infected macrophages is idiosyncratic to TB10.4$_{4-11}$-specific CD8 T-cells, we determined whether CD8 T-cells specific for other Mtb epitopes would recognize Mtb-infected macrophages. To address this question, we focused on a second well-described antigen recognized by CD8 T-cells, the Mtb32A protein (i.e., Rv0125)[30,31]. The CD8 T-cell response to Mtb32A$_{309-318}$ is subdominant to TB10.4$_{4-11}$-specific CD8 T-cells, but accounts for a significant fraction of lung CD8 T-cells in the Mtb-infected lung early after vaccination. Polyclonal CD8 T-cell lines were generated from C57BL/6 mice vaccinated with the Mtb32A$_{309-318}$ epitope followed by repeated *in vitro* stimulation with the peptide. Following two rounds of stimulation, 90% of the T-cell line stained with a K^{b}/Mtb32A$_{309-318}$ tetramer [Fig.1A, left]. The Mtb32A-specific CD8 T-cell line produced IFN-γ when cultured with macrophages pulsed with Mtb32A$_{309-318}$ peptide or with γ-irradiated Mtb [Fig.1B, left]. However, like TB10.4-specific CD8 T-cells, it failed to recognize to Mtb-infected macrophages.

Using the same approach, we generated a second polyclonal CD8 T-cell line (hereafter referred to as DM108) specific for TB10.4$_{20-28}$, which is an immunodominant epitope in Mtb-infected BALB/c mice and presented by H-2 K^{d} [Fig.1A, right]. The DM108 CD8 T-cell line produced IFN-γ when cultured with macrophages pulsed with TB10.4$_{20-28}$ peptide or γ-irradiated Mtb, but not Mtb-infected macrophages [Fig.1B, right]. These data show that inability of Mtb-infected C57BL/6 macrophages to present TB10.4$_{4-11}$ to MHC-I-restricted CD8 T-cells is not idiosyncratic, as the same phenomenon is observed for CD8 T-cells specific to different antigens and occurs in different genetic backgrounds (i.e., BALB/c).

Infected macrophages cross-present antigen but fail to activate Mtb-specific CD8 T-cells.

The poor recognition of infected macrophages by Mtb-specific CD8 T-cells raised the possibility that infected macrophages inefficiently cross-present phagosomal antigens by class I MHC. While XPT has primarily been characterized in DC, there is evidence that macrophages cross present as well[23]. To assess the ability of thioglycolate-elicited peritoneal macrophages (TGPM) to cross-present antigen, we added TB10.4 protein-coated beads to TGPM and then added TB10.4-specific CD8 T-cells. TB10.4-bead-treated TGPM activated the RG3 TB10.4-specific CD8 T-cell line[27,29], in a dose dependent manner, verifying the capacity of TGPM to cross-present antigen [Fig.2A].

TGPM can cross-present TB10.4 to CD8 T-cells, whether the antigen is coated onto beads [Fig.2A] or in the form of γ-irradiated Mtb[29]. TGPM infected with TB10.4-expressing *Listeria monocytogenes* (Lm) present the $TB10.4_{4-11}$ epitope to RG3 CD8 T-cells, by a listerolysin (LLO) dependent pathway. Under these conditions, TB10.4 can access the cytosol and be presented by the canonical MHC I pathway [Fig.S1]. Thus, we conclude that TGPM can use both the canonical and XPT pathways to present TB10.4 to CD8 T-cells. The extensive data by us and others showing that macrophages can cross-present antigens led us to hypothesize that live Mtb infection globally inhibits XPT. We reasoned that if Mtb infection globally inhibits XPT, MHC I presentation of ovalbumin (OVA) coated beads would be impeded. Uninfected macrophages or macrophages infected with Mtb or fed γ-irradiated Mtb were pulsed with OVA-coated beads and then cultured with the $OVA_{257-264}$-specific RF33.70 T-cell hybridoma [32]. All conditions led to the activation of the RF33.70 based on IL-2 secretion, showing that Mtb did not interfere with the ability of TGPM to cross-present antigen [Fig.2B].

An alternative hypothesis is that Mtb infection specifically inhibited XPT within Mtb-containing compartments (MCC), which would explain why OVA-bead presentation was unaffected. To test this possibility, we measured the recruitment of the cellular XPT machinery to MCC by measuring colocalization of XPT markers with H37Rv.YFP-containing phagosomes. Sec22b contributes to the cytosolic pathway of XPT by facilitating trafficking of ER components

into phagosomes[33–35]. We found strong colocalization between Sec22b and Mtb in TGPM, which increased over time with mean Mander's coefficient from 0.26 – 0.54 [Fig.2C], which was higher than Sec22b colocalization with latex beads [Fig.2D]. We found significant colocalization of the XPT markers P97[36,37] and MHC-I, but not the vacuolar component Cathepsin S or early endosome marker Rab5 [Fig.S2]. While unexpected, these results imply that Mtb does not significantly interfere with ER-endosomal vesicular trafficking.

We next tested whether macrophage activation would enhance XPT of Mtb antigens to T-cells. Pre-activating macrophages enhances their phagocytic and antigen presentation capacity [38,39], and while Mtb infection alone does stimulate TLR signaling[40,41], we wondered if other activation pathways and pre-activation might enhance XPT in macrophages. We found that activating TGPM with LPS enhanced their presentation of OVA-coated beads to the RF33.70 CD8 T-cell hybridoma, while IFN-γ had a small but not statistically significant effect [Fig.2E]. Extension of these treatments to Mtb-infected macrophages did not enhance XPT to RG3 cells [Fig.2F]. IFN-γ pre-treatment slightly enhanced presentation of TB10.4 by protein-coated beads but not by Mtb-infected macrophages [Fig.2G].

DC more efficiently cross-present antigen to CD8 T-cells than macrophages[20,23]. Therefore, we considered whether Mtb infection of bone-marrow (BM) derived DC (BMDC) or HoxB8 differentiated DC [42,43] might activate CD8 T-cells. These DC, like the experiments with macrophages, did not activate TB10.4-specific CD8 T-cells [Fig.S3]. The cDC1 subset most efficiently cross-presents antigen to CD8 T-cells, and in vitro derived BMDC more closely resemble cDC2. To assess whether cDC1 play a role in priming of TB10.4-specific CD8 T-cells, we used Batf3$^{-/-}$ mice, which have a developmental deficiency of cDC1[44]. The number of pulmonary TB10.4- and 32A-specific CD8 T-cells was similar in Mtb-infected Batf3$^{-/-}$ and B6 mice indicating that Batf3-dependent DC are not required for priming CD8 T-cell responses to these immunodominant Mtb antigens [Fig.S4]. We suggest that a different type of APC is priming these responses, or there is compensatory development of CD8α^{+} DC during Mtb

infection[45]. These results suggest that Mtb does not appear to globally interfere with XPT in macrophages or DC, but that the Mtb-containing phagosomes avoid XPT to CD8 T-cells under conditions that permit presentation to CD4 T-cells.

High intracellular bacterial burden leads to cross-presentation

Our lab determined that only low frequencies of polyclonal CD4 or CD8 T-cells isolated from the lungs of infected mice recognize Mtb-infected macrophages *in vitro,* as detected by IFN-γ production[10,28,29,46]. These data were obtained using conditions that included infecting macrophages with Mtb for an extended time, which contrasts with the two-hour infection protocol previously used by us and others[29,47–50]. A disadvantage of an overnight infection is that highly infected macrophages are more likely to undergo necrosis; however, we previously identified conditions and an MOI that minimized cell necrosis[46]. We revisited this issue to determine how varying the MOI overnight affects macrophage cell death. As expected, increasing the number of Mtb added to macrophages (i.e., the MOI) for 24 hours correlated with cell death [Fig.3A, left]. By determining the number of intracellular Mtb, we calculated a corrected MOI adjusted for cell death [Fig.3A, middle and right]. These results suggest that despite massive cell death, there exist populations of highly infected macrophages at the highest MOIs.

Determining the number of Mtb CFU recovered from infected macrophages culture allows one to calculate an average MOI. However, we expect there to be considerable heterogeneity in Mtb infection at the individual cell level. Using an experimental approach that enabled image analysis of all macrophages in each condition, we compared macrophages infected for two hours or 24 hours, at several different MOI, with H37Rv.YFP. We quantified the pixels of H37Rv.YFP in each macrophage and inferred the apparent bacteria/macrophage ratio [Fig.3B]. After the standard two-hour (low MOI) infection, 16-27% of the macrophages were infected, and those that were had a median of 2.0-2.3 Mtb/macrophage [Fig.3C, D]. Overnight

(high MOI) infection led to infection of 79-86% of macrophages, with a median of 6.3-12.4 Mtb/macrophage. As expected, we found that after overnight infection with high MOIs, there was significant heterogeneity in the macrophage bacterial burden [Fig.3C, D].

We next asked how these two different infection conditions affected antigen presentation to CD4 and CD8 T-cells. The DM108 CD8 T-cell line recognized macrophages infected at a high MOI but did not recognize macrophages infected at low MOIs [Fig.3E]. Similarly, RG4 CD8 T-cells specifically recognized B6 macrophages infected for 24 hours but not 2 hours [Fig.3F, right]. As reported previously, P25 CD4 T-cells did recognize low MOI infected macrophages but recognized the high MOI infected macrophages more robustly [Fig.3F, left]. Neither RG4 nor P25 produced IFN-γ when cultured with Mtb-infected BALB/c (i.e., H-2 mismatched) macrophages. This demonstrates that T-cell production of IFN-γ when cultured with Mtb-infected B6 macrophages was H-2 restricted and not the result of noncognate activation (e.g., cytokine mediated stimulation). Thus, both at a low and high effective MOI, Mtb-infected macrophages more efficiently presented antigen to CD4 T-cells than CD8 T-cells. We occasionally observed that CD4 T-cells, and to a lesser extent CD8 T-cells, would not respond at the highest MOI in some experiments, which we attributed to the number of viable APC falling below a critical threshold secondary to cell death (Fig.S5).

Based on these data, we hypothesized that CD8 T-cells preferentially recognize highly infected cells. To measure CD8 recognition of Mtb-infected macrophages independently of IFN-γ production, we cultured H37Rv**.**YFP-infected macrophages with RG4 CD8 T-cells and measured stable interactions between T-cells and Mtb-infected macrophages. Images were captured by immunofluorescence microscopy and Strataquest imaging analysis software was used to identify macrophages, quantify their bacterial content, and enumerate T-cell contacts. We leveraged the heterogeneity of the *in vitro* infection to determine the propensity of CD8 T-cells to interact with macrophages over a range of MOIs. Few CD8 T-cells interacted with uninfected or low MOI (i.e., 1 or 2) infected WT or MHC $I^{-/-}$ macrophages [Fig.3G]. However, as

the MOI increased, significantly more T cells interacted with Mtb-infected WT macrophages compared to MHC $I^{-/-}$ macrophages. This preference was observed between a range of MOI = 3-18 [Fig.3G, 3H]. Furthermore, the mean T-cell contacts with infected WT HOXB8 macrophages was significantly correlated with intracellular bacilli (Spearman ρ= 0.19, $p<0.0001$). In contrast, there was no correlation between T-cells interacting with MHC $I^{-/-}$ macrophages and the number of intracellular Mtb (Spearman ρ= 0.0236, p=n.s.). These data confirm that T-cell-macrophage interactions are TCR-MHC dependent, and taken together, support the hypothesis that CD8 T-cells preferentially recognize highly infected macrophages and poorly recognize macrophages containing few bacilli.

Cell death correlates with cross presentation

Why a high bacterial burden should drive MHC I presentation was not intuitively obvious. We had previously argued that the inability of macrophages to present TB10.4 was not an issue of antigen abundance[29]. In considering possible mechanisms, we considered the correlation between the conditions that led to significant cell death of infected macrophages and those that promoted MHC I presentation [Fig.3A] and hypothesized that cell death promotes XPT of Mtb antigens[48,51–55]. We previously demonstrated that Mtb-infected apoptotic macrophages are engulfed by other macrophages and skewing of infected macrophage death towards apoptosis is associated with better CD8 and CD4 T-cell priming[51–53]. Mtb-infected macrophages die primarily by necrosis[51,52,54], which is enhanced by high bacterial burdens[55–57], and these necrotic macrophages are also engulfed by other phagocytes[58,59]. Therefore, we envisioned that antigen could be transferred from dying cells to nearby cells that secondarily present them to CD8 T-cells (indirect XPT). To test this possibility, we used Celltracker™ dyes to differentiate between primary infected (Deep Red) and uninfected bystander (VioGreen) macrophages [Fig.4A]. Under these conditions, between 2-6% of the bystander macrophages contained H37Rv.YFP, indicating that they are secondarily infected [Fig.4B, left]. Of the secondarily infected

macrophages, 75-83% acquired Deep Red dye from the primary-infected macrophages [Fig.4B, right]. These data indicate that the majority of "secondarily infected" macrophages acquire Mtb following phagocytosis of dying infected macrophages. These findings were confirmed by immunofluorescence microscopy [Fig.4C], and we identified a strong correlation between uptake of Mtb and primary-infected macrophages (Deep Red) by bystander macrophages (R^2 = 0.4375) [Fig.4D]. Based on these results, we conclude that high MOI Mtb infections drive host cell death, and bystander macrophages effectively phagocytose dead cellular debris and Mtb.

We next determined the relative contributions of direct presentation from infected macrophages versus indirect XPT by bystander macrophages that secondarily acquired antigen. We established an antigen transfer assay that mimics what could occur in the lung, where there are relatively few infected macrophages, often surrounded by uninfected myeloid cells. WT or MHC $I^{-/-}$ macrophages were infected for 24 hours, and extensively washed to remove any extracellular bacilli. Then, uninfected WT or MHC $I^{-/-}$ macrophages and TB10.4-specific CD8 T-cells were added, and IFN-γ was measured after 24 hours [Fig.4E]. To establish the baseline of non-cognate activation of the CD8 T-cells, MHC $I^{-/-}$ macrophages and T-cells were added to infected MHC $I^{-/-}$ macrophages ["K/K," Fig.4F]. As the MOI, was increased, a small but significant amount of IFN-γ was produced compared to the uninfected condition (i.e., MOI = 0). To determine the degree of direct XPT by primary-infected macrophages, uninfected MHC $I^{-/-}$ macrophages and T-cells were added to infected WT macrophages. Under these conditions, IFN-γ increased as the MOI was increased, but did not become statistically significant compared to the "K/K" group until an MOI=8 ["W/K," Fig.4F]. In contrast, the greatest amount of IFN-γ was produced when uninfected WT macrophages were added to infected cells, regardless of their genotype of the primary infected macrophage (i.e., WT or MHC $I^{-/-}$) [see "W/W" and "K/W," Fig.4F]. These results suggest that during high MOI infection, antigen transfer to bystander cells leads to indirect XPT to CD8 T-cells.

We next assessed whether soluble antigen or antigen-laden vesicles released by infected macrophages could be the source of Mtb antigen taken up by the bystander macrophages and presented to CD8 T-cells. To test this possibility, we collected supernatants from macrophages infected overnight. Addition of these unfiltered supernatants neither conferred nor enhanced presentation by uninfected or infected macrophages, respectively [Fig.4F]. Although free antigen, or even vesicles may be diluted in vitro so they are less bioactive, our results suggest that efficient antigen transfer requires intact cells. We envision that engulfment of dying infected cells could result in concentration of antigen in a presentation-competent compartment[53,60]. Based on these data, we conclude that indirect XPT by uninfected macrophages enhances CD8 T-cell activation during Mtb infection.

The ESX-1 type VII secretion system is required for cross presentation

Our finding that CD8 T-cell activation requires high MOI infection and is associated with macrophage death or occurs when uninfected macrophages cross-present Mtb antigens, suggests that cell death of infected macrophages is a prerequisite for XPT of Mtb antigens. As the ESX-1 type VII secretion system is a major virulence factor that disrupts the phagosomal membrane and induces cell necrosis[61,62], we hypothesized that ESX-1 would be required for MHC I presentation by macrophages. To test this possibility, we compared CD8 T-cell recognition of macrophages infected with wild-type H37Rv and a Mtb mutant with a deleted RD1 locus (ΔRD1), which removes most of the genes required for ESX-1 function[62,63]. Macrophages infected with the ΔRD1 mutant or H37Rv had similar intramacrophage bacterial burdens [Fig.5A, Left]. However, macrophages infected with the ΔRD1 mutant had little or no cell death compared to H37Rv-infected macrophages, either at 24 hours (i.e., when T-cells are added for the assay) or at 48 hours (i.e., when IFN-γ is measured) [Fig.5A, center and right]. The inflated viability of ΔRD1-infected macrophages results from staining of Mtb by crystal violet. Remarkably, infection with ΔRD1, even at high MOIs, did not lead to XPT and failed to activate

TB10.4-specific CD8 T-cell lines [Fig.5B, 5C]. In contrast, ΔRD1- and H37RV-infected macrophages were both recognized by Ag85b-specific CD4 T-cells [Fig.5D]. Interestingly, CD4 T-cell activation was diminished at the highest MOI of H37Rv-infected but not ΔRD1-infected macrophages, which we suggest is due to APC death induced by fully virulent Mtb.

As the ΔRD1 mutant is difficult to complement and may have other defects, we validated our results by disrupting the PhoPR regulon (ΔPhoPR), which is required for the expression of the ESX-1 secretion system, in H37Rv[56,64–66]. CD8 T-cells were not activated by ΔPhoPR-infected macrophages [Fig.5E]. In contrast, TB10-specific CD8 T-cells were activated by macrophages infected with the ΔPhoPR::PhoPR complemented strain Thus, ΔPhoPR phenocopies the ΔRD1 strain and can be complemented, which confirms that the ESX-1 type VII secretion system is required for XPT of Mtb antigens by MHC I.

Activation state of TB10.4-specific CD8 T-cells in the lungs of Mtb-infected mice

To characterize the activation status of CD8 T-cells ex vivo, flow sorted lung parenchymal T-cells (i.e., IV-CD45^{-}) from mice 6- and 41-weeks post infection (wpi) were analyzed by single cell RNAseq. After filtering to exclude dead cells and doublets from analysis, 2,349 CD8 T-cells from 6 wpi, and 6,605 CD8 T-cells from 41 wpi were analyzed. Paired TCRs were identified for 1,900 (80.9%) and 4,390 cells (66.5%), respectively. The TCR genes were excluded to permit clustering of the cells based on function and we used an integrated analysis to identify and compare the common cell states 6 and 41 wpi. Nine clusters of CD8 T-cells were identified (Fig.6A, Fig.S6, S7A, Table S1). A spectrum of cellular states was detected including naïve (cluster 4), cycling (cluster 6), effector and polyfunctional (cluster 0, 7), and exhausted (cluster 1) CD8 T cells. CD8 T cells with a type I IFN signature (cluster 8) which expressed high levels of ISG15, IFIT1, IFIT2, and IRF7, were identified, like CD4 T cells from the lungs of HN878-infected mice [67] . GLIPH2 analysis identified the “RENS” motif as a dominant specificity group, which was restricted to CDR3β sequences of a similar length and shared V gene

distribution as we had previously described for K^b-restricted TB10.4_{4-11}-specific CD8 T-cells with the “DRENSD” motif[26,27]. We defined TB10.4-specific CD8 T-cells by using the “RENS” motif instead of the “DRENSD” motif as it captured an additional conserved TCR (CDR3β, “CASSRNRENSDYTF”). This TCRβ paired with a TCRα chain with the CDR3α motif “CAVSGGGRALIF,” which we previously associated with TB10.4-specific CD8 T-cells[29]. It is striking that TCRs with the CDR3β “RENS” motif dominated the CD8 T-cell response at 6 and 41 wpi (Fig.6B, C, D). Nine distinct CDR3β regions used the “RENS” motif (Fig.6E). We identified independent recombination events that generated the “RENS,” indicating clonal expansion and convergent recombination (Table S2)[68,69]. Six of the 12 associated TCRα chains have a CDR3α sequence of “CAVSxGGRALIF”, where x=E, G, M, Q, S, W (Fig.6F, Fig.S7B). Thus, CD8 T-cells with the CDR3β “RENS” motif underwent massive clonal expansion during Mtb infection based on the sharing of identical TCRα VJ and TCRβ VDJ recombination sites. This is also supported by enrichment of TCR signaling genes in CD8 T-cells with the “RENS” motif (Fig.S7C). Furthermore, the CDR3α chain appears to be co-selected. These features indicate that the TB10.4-specific CD8 T-cell response is driven by antigen selection. CD8 T-cells with the “RENS” motif were found all 9 clusters except for the “naïve” cluster (cluster 4), which consisted of CD8 T-cells that were not clonally expanded (Fig.6B). During chronic infection (i.e., 41 wpi), the TB10.4-specific TCRs dominated the activated cluster (cluster 0) and were sparsely represented among exhausted and resident memory-like cells (clusters 1 and 3, respectively) (Fig.6B).

Six weeks after infection, Ifng and Tnf RNA levels in “RENS” CD8 T-cells were like other clonally expanded CD8 T-cells (Fig.6G, Table S3). Ccl4, Ccl5, and Gzmb were expressed more in non-“RENS” clonally expanded CD8 T-cells (Fig.6H). By 41 wpi, Cluster 0, which contained the most TB10.4-specific CD8 T cells, also had the greatest ‘Effector-like’ signature (Fig.6I). The function of “RENS” vs. other clonally expanded CD8 T-cells diverged at 41 wpi. “RENS” CD8 T-cells were more activated and expressed more Ifng, Tnf, and other genes associated with

effector activity (Fig.6J, Table S3). Other significant transcriptional differences emerged during chronic infection. Gene Ontology analysis showed enrichment of pathways involved in cell signaling and cell interactions (Fig.S7D). In contrast, other clonally expanded CD8 T-cells were more likely to be exhausted based on expression of Pdcd1, Tigit, Lag3, and Tox (Fig.6I, J). These data indicate that TB10.4-specific CD8 T-cells participate in the immune response against Mtb infection and adopt a variety of transcriptionally defined states. Thus, late during Mtb infection (i.e., 41 wpi), TB10.4-specific CD8 T-cells account for a greater proportion of CD8 T-cells in the lung and are more likely to be activated and resist exhaustion than other expanded CD8 T-cells.

Discussion

These studies expand upon our key observation that TB10.4-specific CD8 T-cells poorly recognize Mtb-infected macrophages and shows that inefficient MHC I antigen presentation by infected macrophages is a general phenomenon. Importantly, all the diverse types of macrophages used in this study can cross-present non-viable antigen to CD8 T-cells. Our results confirm that Mtb does not globally inhibit MHC I antigen presentation [32]; instead, our data points to a defect specific to mycobacteria-containing compartments. Importantly, we do not believe that the poor recognition of infected macrophages is a feature only of the CD8 T-cell lines used in this study: only 10% of polyclonal CD8 and 15-20% of polyclonal CD4 T-cells from the lungs of infected mice produce IFN-γ when cultured with Mtb-infected macrophages [28,46].

Here, we identify conditions that permit more efficient MHC I presentation of Mtb antigens to CD8 T-cells. *In vitro* infection of macrophages for 24 hours led to significantly more intracellular Mtb than a standard two-hour infection. More highly infected macrophages gain the capacity to present MHC I-restricted Mtb epitopes to CD8 T-cells. These data are consistent with work from the Lewinsohn lab showing that human CD8 T-cell clones preferentially recognized highly infected human DCs [70]. In contrast to CD8 T-cells, CD4 T-cells are activated even at a low MOI. Why is a high intracellular Mtb burden required for MHC I antigen presentation? One might assume that more bacilli lead to more antigen. However, we do not believe that antigen quantity is the key factor. We previously showed that overexpression of TB10.4 does not enable CD8 T-cell recognition of macrophages infected at low MOIs [29]. Also, if this were only an issue of antigen abundance, high MOI infections of macrophages with Mtb strains containing deletions of the RD1 locus or the PhoP gene should be recognized by TB10.4-specific CD8 T-cells.

A high bacterial burden promotes cell death primarily through necrosis [52,54–57]. We and others have shown that macrophages engulf dying infected cells [53,71,72], and it is well established that DC can engulf dead, antigen-bearing cells and cross-present their antigens [73–76]. Therefore,

we explored the possibility that dying infected cells were a source of Mtb antigens to bystander macrophages to enhance MHC I presentation (i.e., indirect XPT). Bystander macrophages efficiently acquired antigen from highly infected cells and cross-presented this antigen to CD8 T-cells. This indirect XPT stimulated CD8 T-cells even more so than primary infection alone. Based on the design of these experiments, it is possible that indirect XPT is the dominant pathway that activates CD8 T-cells as we cannot exclude the possibility that primary-infected macrophages also engulf dying infected macrophages and cross-present the bacterial antigens. Cell death directly contributes to high bacterial burden by facilitating bacterial growth, and reuptake by bystander macrophages, creating a cycle of increasing Mtb burden and necrosis [58,59]. However, we cannot rule out the occurrence of direct antigen presentation. Furthermore, we hypothesize that indirect presentation requires direct contact with dead/dying cells since we did not observe XPT after supernatant transfer. Thus, efferocytosis or phagocytosis may engulf dying infected cells, leading to the concentration of Mtb antigens, which are shuttled to XPT-competent endosomes by scavenging receptors as has been shown for DNGR1 in DC [75–77].

The ESX-1 type VII secretion system, which is encoded within the RD1 locus, is one of the key virulence factors of Mtb and can cause phagosomal membrane damage [61,62,78]. We show that ESX-1 is necessary for MHC I presentation of Mtb antigen by infected macrophages. While we believe that ESX-1-associated macrophage death is the major pathway that licenses XPT, there are alternative hypothesis to consider. ESX-1 mediated phagosomal membrane damage could enable Mtb antigens access to the macrophage cytosol and facilitate MHC I presentation to CD8 T-cells. A high bacillary burden could be required for sufficient production of ESX-1 complexes to make the phagosomal membrane permeable to Mtb antigens. Cytosolic Mtb is sensed by cytosolic surveillance pathways including STING [40,79], which may augment XPT of Mtb antigens. Finally, we favor the idea that activation of cell death pathways of Mtb-infected macrophages, leads to their engulfment by bystander macrophages. Skewing of cell death towards apoptosis will lead to efferocytosis and is associated with enhanced CD8 T-cell

responses [52,54,80]. While some macrophages infected with virulent Mtb will undergo apoptosis, many more are thought to undergo necrotic cell death. In this study, we did not define the mode of cell death, as both apoptotic and necrotic cells are engulfed by phagocytes [72,75,81,82]. Interestingly, we previously reported that ESX-1 is not required for in vivo priming of TB10.4-specific CD8 T-cells [83]. The disparity between the requirements for initial CD8 T-cell priming and recognition of infected macrophages at sites of infection could reflect that in vivo, death of macrophages by apoptosis (more frequent in the absence of ESX-1) and necrosis (more frequent in the presence of ESX-1) both ultimately lead to acquisition of Mtb antigens by APC.

The observation that CD8 T-cells respond to highly infected macrophages sheds light on our previous *in vivo* observations. It is paradoxical that TB10.4-specific CD8 T-cells don't recognize infected macrophages in vitro but are a dominant and persistent populations in the lungs of infected mice. There is an interesting discrepancy in the capacity of TB10.4-specific CD8 T-cells to mediate protection. Vaccination with TB10.$4_{4\text{-}11}$ peptide does not protect mice against Mtb challenge, nor do TB10.4-specific CD8 T-cells enhance the ability of infected macrophages to control Mtb replication [26,29]. However, Mtb-infected TCR$\alpha^{-/-}$ mice control Mtb infection better after transfer of TB10.4-specific CD8 T-cells and their protection is TAP1-dependent [27]. We now surmise that in immunodeficient mice, the bacterial burden becomes so high that the transferred CD8 T-cells are activated by indirect XPT, which as the main source of IFN-γ, protects the lungs. Interestingly, even in immunocompetent mice, CD8 T-cells with the "RENS" clonotype (i.e., TB10.4-specific CD8 T-cells) include ones that are highly proliferative (i.e., Cluster 6), suggesting stimulation via TCR signaling. Also, these CD8 T-cells are highly activated late during infection and are overrepresented in Cluster 0 (activated) and underrepresented in Cluster 1 (exhausted). As Il18r1 and Il18rap are upregulated by these CD8 T-cells at 41 wpi (Fig.6J, Table S3), their highly activated state is likely to be driven by a combination of TCR signaling and IL-12 and IL-18, as observed for NKT cells and memory CD8 T-cells[48,84]. Both the bystander activated T cell gene signature [85] and TCR signaling gene sets in

MSigDB-GSEA were upregulated in RENS-motif at 41 wpi. Our detailed single cell transcriptional analysis of CD8 T cells ex vivo shows that they adopt a spectrum of cellular activation states. After eliminating intravascular cells, we identify naïve, proliferating, effector and exhausted CD8 T cells. CD8 T cells in cluster 8 had a signature of IFN-stimulated CD8 T cells, identified by the expression of IFN-regulated genes such as Ifit1, Bst2, Isg15, and Irf7, as has been described by Akter, Chauhan, et al for CD4 T cells [67]. Few genes associated with canonical effector function (i.e., Ifng, Prf1, etc.) were expressed in cluster 8. A possible causal link between type I IFN signaling and T cell exhaustion is being explored [86,87], and we observed enrichment of a co-inhibitory gene signature [88] in this cluster (Fig.S7A).

If indirect XPT activates Mtb-specific CD8 T-cells in the lung during active TB, MHC I presented antigens could act as decoy antigens. CD8 T-cell recognition of Mtb antigens presented by uninfected APC could promote inflammation and promote Mtb transmission. In this scenario, the activated CD8 T-cells would have little impact on the outcome of infection. On the other hand, mediators (e.g., IFN-γ and TNF) released by CD8 T-cells activated by indirect XPT could activate nearby infected macrophages. CD8 T-cells might be important in mediating protection when there is significant bacterial growth and other immune mechanisms are failing. Recent work in rhesus macaques shows that CD8 T-cells contribute to protection late during infection [89] and CD8 T-cells are associated with granulomas that control Mtb infection in cynomolgus macaques [90]. Pre-existing (i.e., vaccine-elicited) Mtb-specific CD8 T-cells could also play a role early during infection when the intracellular bacillary burden can exceed 20 bacilli/monocytic cells in the lung [57]. However, our data predicts that this function could be equally performed by CD4 T-cells. An important issue to consider is whether certain antigens are more likely to be directly cross-presented by Mtb-infected macrophages, as such antigens might be more effective in focusing the CD8 T-cells response on infected macrophages instead of uninfected bystander cells that have acquired Mtb antigens. We predict that developing approaches to distinguish Mtb antigens that are directly cross-presented by infected

macrophages from those that are indirectly cross-presented would empower target selection for vaccines that elicit protective CD8 T-cells.

Methods and Materials

Ethics Statement

Studies were conducted using the relevant guidelines and regulations and approved by the Institutional Animal Care and Use Committee at the University of Massachusetts Chan Medical School (UMMS) (Animal Welfare A3306-01), using the recommendations from the Guide for the Care and Use of Laboratory Animals of the National Institutes of Health and the Office of Laboratory Animal Welfare.

Aerosol Mtb Infection of Mice

Mice were infected by the aerosol route as previously described (Lee et al., 2020). Frozen bacterial stocks were thawed and diluted into 5 mL of 0.01% Tween-80 in PBS, then sonicated to create a bacterial suspension. Mice were infected with ~100 CFU Mtb Erdman via the aerosol route using a Glas-Col airborne infection system.

Intravascular Staining

Mice were injected intravenously with 2.4 µg/mouse of anti-CD45 – BV750 in 200 µL of injection medium (2% FBS in PBS) 2 minutes before euthanizing with CO_2. Lungs were then perfused and removed 3 minutes after anti-CD45 injection. Lymphocytes from blood collected in RPMI containing 40 U/mL of heparin were isolated using Lympholyte (CEDARLANE) and analyzed by flow cytometry to confirm uniform staining with anti-CD45 – BV750.

Generation of single-cell suspensions from tissues

Lung single-cell suspensions from Mtb infected mice were isolated as previously described (Lu et al., 2021). Briefly, mice were euthanized with CO_2 and lungs were perfused with 10 mL RPMI (GIBCO) before harvest. Single cell suspensions were prepared by homogenizing lungs using a GentleMACS tissue dissociator, digesting with 300 U/mL collagenase (Sigma) in complete RPMI (10% FBS, 2mM L-Glutamine, 100 U/mL Penicillin/Streptomycin, 1 mM Na-Pyruvate, 1X non-essential amino acids, 0.5X Minimal essential amino acids, 25 mM HEPES, and 7.5 mM NaOH) at 37C for 30 minutes, and followed by a second run of dissociation using the GentleMACS. Suspensions were then filtered through 70 µm strainers and incubated with 1 mL ACK Lysis Buffer (GIBCO) for 1 minute at room temperature (25C). The cells were resuspended in suitable media or buffer for further use and filtered through 40 µm filters.

Macrophages and DC

Thioglycolate elicited peritoneal macrophages (TGPM) were harvested by first injecting mice with 2 ml of 3% thioglycolate broth intraperitoneally. 4-5 days after injection, macrophages were extracted through peritoneal lavage and purified with Miltenyi Biotec CD11b microbeads (Catalog #130-049-601). HOXB8 progenitor cells were established as described [91]. MHC I KO lines were generated with bone marrow from the β2 microglobulin knockout line B6.129P2-B2mtm1Unc/DcrJ (Jackson). Progenitor cells were collected, washed twice with PBS, and cultured in 150 x 15 mm non-adherent plates in the appropriate media. For macrophages, progenitors were cultured in 20% L929 media for 8-12 days before adherent cells were harvested. DC were cultured in either 10% GM-CSF or 5% FLT3 as indicated in the results. BMDC were prepared as previously described [92]. Briefly, bone marrow harvested from murine femurs was washed and cultured in 10% GM-CSF complete media for 10 days. Non-adherent cells were harvested and used for infections.

Protein-coated beads

BioMag®Plus Amine protein coupling kit (Bangs Laboratories Inc.) (Catalog #86000-1) was used to conjugate full length Ovalbumin (Sigma-Aldrich #A5503) or TB10.4 (manufactured by Genscript) protein to magnetic beads according to the manufacturer's protocol. Briefly, BioMag®Plus Amine particles were washed, activated, and magnetically separated before being incubated with protein for conjugation. The beads were further washed, and the reaction was quenched before being diluted for use in assays.

Infections

Mycobacterium tuberculosis strains were cultured in Middlebrook 7H9 broth until an OD_{600} of 0.8-1.2 was reached. Cultures were washed by centrifugation and incubated in TB coat (1% FBS, 2% human serum and 0.05% Tween-80 in RPMI) for 5 minutes to opsonize bacteria and impede clumping. Bacteria were washed again and resuspended in complete media without antibiotics. Suspensions were filtered through a 5 µm filter to remove clumps and absorbance was measured to estimate bacterial density. Diluted Mtb was added to target cells at the corresponding MOI and left for 2 (low MOI infections) or 18 – 24 (high MOI infections) hours at 37°C. Cells were then washed 3-4 times with warm RPMI to remove extracellular bacteria.

ΔphoPR mutant and complementation

The ΔphoPR mutant of M. tuberculosis H37Rv was isolated following allelic exchange of 2.178 kb region of the phoP-phoR (rv0757-rv0758) sequence with a hygromycin-chloramphenicol cassette as described previously (Lee et al., 2011). The hygromycin-resistant ΔphoPR mutant retained the first 32 bases of phoP gene and the last 36 bases of the phoR gene. For complementation, a 3.3 kb DNA fragment containing the wildtype allele of H37Rv phoPR coding sequence and 1 kb upstream region encompassing the putative promoter was amplified by PCR and cloned into the kanamycin mycobacterial L5 attB integrating vector pMV306 (MedImmune

Inc., Gaithersburg, MD) to construct the phoPR complementing plasmid pKP406. Following sequence verification of the cloned insert, the KanR plasmid pKP406 was electroporated into the hygromycin-resistant M. tuberculosis ΔphoPR mutant and the transformants were selected on 7H10 plates supplemented with 50 µg/ml hygromycin and 25 µg/ml kanamycin.

Polyclonal T-cell lines

Mice were vaccinated using the Trivax vaccination strategy[93] with either TB10.4$_{20-28}$ or Mtb32A-$_{309-318}$ two to three times, three weeks apart, as previously described[26]. The frequency of antigen specific CD8 T-cells was estimated by flow cytometry after staining peripheral blood with the Mtb-specific tetramers K^b/Mtb32A$_{309-318}$ and K^d/ TB10.4$_{20-28}$ provided by the NIH Tetramer Core. Mice with positive vaccine responses were euthanized to allow collection of the spleens and peripheral lymph nodes. CD8 T-cells were isolated using Stem Cell CD8 isolation kits (Catalog #19753). Purified CD8 T-cells were cultured with peptide-pulsed irradiated splenocytes to activate and expand antigen-specific CD8 T-cells. The polyclonal cells were successively restimulated using irradiated splenocytes, peptide, and IL-2, every 4 weeks to expand and enrich antigen-specific populations. Antigen-specific CD8 T-cells were quantified using tetramers supplied by the NIH tetramer core.

T-cell recognition assays

Macrophages were seeded in 96 well float bottom TC-treated plates at a density of 100,000 cells/well and infected as described above. T-cells were added to infected macrophages in a 1:1 ratio unless noted otherwise. For ELISA analysis, supernatants were collected after co-culturing the cells for 24 hours at 37°C. Supernatants were filtered through 0.2 µm filter plates to exclude any bacteria, and cytokine levels were quantified with Biolegend ELISA kits (Catalog #430801). For flow cytometry, T-cells were co-cultured with infected macrophages for 6 hours at 37°C with

brefeldin A (Golgiplug). Cells were then stained for surface markers and intracellular cytokines as described [10].

Immunofluorescence microscopy staining

T-cells were cocultured with infected macrophages for the time indicated. Samples were washed with PBS and fixed with 4% paraformaldehyde for 20 minutes. Samples were washed with PBS and blocked in 1% BSA for 30 minutes at room temperature. Samples were then washed and incubated in the appropriate primary antibodies overnight at 4°C. Cells were then washed and incubated in secondary antibody for one hour at room temperature.

Fluorescent beads for confocal microscopy

We used Polysciences Fluoresbrite® YG Microspheres 3.00µm for confocal imaging analysis. Beads were washed in PBS with 1% BSA, then opsonized with TB coat (1% FBS, 2% human serum and 0.05% Tween-80 in RPMI) at room temperature for 30 minutes to facilitate phagocytosis. Beads were diluted to 5 x 10^6 beads/ml and added alongside H37Rv Mtb for cell infections.

Confocal imaging and analysis

Images were acquired on a Leica SP8 confocal microscope at on an Apo TIRF 60x Oil DIC N 2 objective with a numerical aperture of 1.49. We used 405, 488 and 640 nm lasers, and 450/50 nm and 525/50 emission filters. Pixel size is 207 x 207 nm, and the voxel depth is 400 nm. 18-24 Z-steps were acquired for each image with a step size of 0.4 µm. Colocalization of targets with Mtb were quantified with ImageJ by calculating Mander's coefficients (Fraction of overlapping pixels between two channels) of the signal of interest with Mtb YFP signal. Regions of interests (ROIs) were manually selected around individual bacilli before coefficients were calculated to quantify the amount of colocalization of our target with Mtb on a cell-cell basis.

Slide scanning Immunofluorescence

Images were acquired with a TissueFAXS iQ tissue cytometer (TissueGnostics GmbH) built on a Zeiss AxioImager.Z2 microscope base with Märzhäuser stage, Lumencor Spectra III light engine, Zeiss EC Plan-Neofluar 20x/0.75 NA objective and Hamamatsu Orca Fusion BT C15440 camera. DAPI filters were 390/22 excitation, 89402 quad dichroic, 89402m emission. AF488 filters were 475/20 excitation, T495lpxr dichroic, ET519/26 emission. TRED filters were 555/28x excitation, 89402bs dichoric, and 89402m emission. Cy5/AF647 filters were 631/28x excitation, 89402bs dichoric, and 89402m emission. AF740/Cy7 filters were 747/11 excitation, T770lpxr and ET810/90m emission.

***Strataquest Image analysis* and quantification**

Whole slide scans were analyzed with Tissuegnostics Strataquest Plus V7.1.1.127 software (TissueGnostics GmbH). We developed analysis pipelines to identify and differentiate T-cells and macrophages based on nuclei identification, staining intensity of F4/80 and CD3, and a cellular mask calculation. Once T-cells and macrophages were identified, we extrapolated total YFP signals for each macrophage to calculate approximate bacterial burdens. We converted the total YFP signal to Mtb numbers by dividing the signal by the average signal of one Mtb bacilli. Next, we also calculated the number of T-cells in contact with each macrophage to correlate Mtb burden with T-cell contacts. Statistical testing including correlations between Mtb burden and T-cell contacts were calculated in GraphPad Prism. We binned macrophages based on their Mtb burden with a bin size of one, then calculated and plotted the mean T-cell contacts of each bin. Between 3100-6900 macrophages were analyzed per condition. MOIs greater than 24 were not analyzed because there were generally fewer than 5 cells in these bins. In contrast, an average of 34 macrophages were analyzed at each MOI between 4-14.

ATP Luciferase viability assay

Cells were infected with Mtb as described above. We used the Abcam Luminescent ATP Detection Assay Kit (ab113849) and followed the provided protocol. Briefly, cells were lysed with detergent for five minutes to release ATP. Substrate was added and incubated in the dark for 15 minutes. Luminescence of the wells was measured, and samples were compared to standards to determine cell viability.

Crystal Violet cell viability

Mtb-infected cells were washed and fixed with 4% paraformaldehyde for 20 minutes at room temperature. Cells were then washed with PBS and incubated with 0.1% crystal violet in water for 30 minutes. Plates were washed by submerging the plate in a container of fresh tap water 3-4 times. Cells were then lysed with 150 µL of 0.2 % Triton X-100 in water for 30 minutes to release crystal violet. Samples were mixed and transferred to a new flat-bottom clear plate and absorbance was measured at 600 nM. Viability was determined as follows: %Viability = ((Ab600 Control – Ab600 Experimental) / Ab600 Control))*100.

CFU determination

Infected macrophages were washed 3X with warm cRPMI to remove extracellular bacteria. Cells were then lysed with 1% Triton X-100 in PBS for 2 minutes. Samples were serially diluted and plated on 7H11 Agar plates from Hardy Diagnostics (Catalog #W40). Plates were incubated at 37°C for 21 days when colonies were counted and Mtb/well was calculated based on the dilutions.

Adjusted MOI calculations

To account for cell death in our Mtb/cell calculations, we calculated the average number of viable cells per condition by multiplying %viability by the number of cells seeded. If the %viability

was quantified at over 100%, we adjusted it to 100%. The number of bacteria/well determined by CFU calculations was divided by the number of viable cells to determine approximate Mtb/cell numbers (# of Mtb / # of cells = Mtb/cell).

Antigen Transfer Assay

B6 WT or MHC I KO macrophages were seeded in 96 well flat bottom tissue culture-treated plates at a density of 50,000 cells/well and infected as described above. Following the infection, 50,000 fresh WT or MHC I KO macrophages were added to the wells along with 100,000 T-cells. Co-cultures were left at 37°C for 16-24 before samples were collected for analysis. Prior to infection, primary-infected macrophages were stained with CellTracker™ Violet BMQC (VioGreen channel) (ThermoFisher # C10094) according to the manufacturer's protocol. The macrophages were infected as described above using the 24-hour ("high MOI") protocol. After extensive washing to remove any remaining extracellular bacteria, bystander (uninfected) macrophages, which had been stained with CellTracker™ Deep Red (ThermoFisher # C34565) to differentiate them from the primary infected macrophages, were added to the culture. The macrophages were cultured for 24 hours, then they were washed and analyzed by flow cytometry or fluorescent microscopy. For microscopy, samples were imaged with the slide scanning software and analyzed with strataquest as described above. Correlations between primary dye and Mtb were calculated and plotted using GraphPad Prism.

Single-cell RNA library generation and sequencing

Anti-CD45 – BV750 (Biolegend) was injected intravenously into mice at 6- and 41-weeks post-infection. The lungs were harvested, and the resulting single cell suspensions were stained with flow antibodies to enrich for total live, parenchymal T-cells (Live/Dead – Zombie Aqua; Biolegend, CD3 – PE/Cy7; Biolegend, CD19 – PE-CF594; BD, TCRgd – PE-CF594; BD, NK1.1 – PE-CF594; BD, TCR-beta – APC/Cy7; Biolegend). scRNAseq was performed on the cells

using Chromium Single Cell 5' (v1 and v2) Reagent Kits as per manufacturer's instructions (10x Genomics). Briefly, sorted cells were resuspended at 1,000 cells/µL in 0.04% BSA in PBS and loaded into the 10x Chromium Controller with the aim to capture 7,000 - 10,000 cells/lane. The resulting suspension contained GEM droplets that underwent reverse transcription where each cell was labeled with a barcode, and each transcript was labeled with a unique molecular identifier (UMI). The cells were removed from the BSL-3 space after reverse transcription for further amplification, gene expression (GEX) library generation, and V(D)J library generation as per the manufacturer's instructions. Libraries were sequenced on a NextSeq 500/550 flow cell with a target of 20,000 reads/cell for GEX and 5,000 reads/cell for V(D)J.

Data Analysis of Single-cell RNA sequencing

Raw sequencing data was demultiplexed and converted into FASTQ using the 10x Genomics Cell Ranger software (version 6.1.2). After demultiplexing, the reads were aligned to the mouse reference genome (GRCm38; 10X Cell Ranger reference GRCm38 v5.0.0), feature-barcode matrices were generated using the CellRanger count. CellRanger aggr command was used to merge the count files of the 8 individual libraries (4 libraries from two 6 wpi mice, 4 libraries from two 41 wpi mice). The merged filtered_feature_bc_matrix was then read into Seurat (v4.1.1) for analysis [94]. The data were filtered to remove cells that expressed <200 genes and genes expressed in less than three cells. We also filtered out the cells that express mitochondrial genes in >10%. Data were normalized using logarithmic transformation normalization. CD8 T-cells were subset based on Cd8a > 0.5 & Cd8b1 > 0.5 & Cd3e > 1 & Cd4 < 1e-10 and we only included this subset for further analysis. We then removed TCR genes (Trav, Traj, Trac, Trbv, Trbd, Trbj, Trbc, Trgv, Trgi, Trgc, Tcrg, Trdv, Trdd, Trdj, Trdc) to remove TCR gene-specific biases and focus on cellular function. The data were then scaled, and principal component analysis (PCA) was performed using top 2000 highly variable genes. Based on the elbow plot, we used the first 15 principal components (PCs) for further analysis. Then, doublet cells were

removed using the R package DoubletFinder (v2.0.3)[95]. We then identified anchors of all libraries using the FindIntegrationAnchors function, and integrated the datasets together with IntegrateData function, create a new integrated matrix. Last, the cells were clustered by unsupervised clustering (0.4 resolution) and visualized by UMAP using the top 15 PCs. Differentially expressed genes (DEGs) were identified using the FindAllMarkers function for each cluster. For each cluster, the minimum required average log fold change in gene expression was set to 0.25 and the minimum percent of cells that must express gene in either cluster was set to 25%. To identify DEGs between the "RENS" motif and Expanded CD8 T-cells, we used FindMarkers functions and genes were considered differentially expressed when the logFC > 0.5 and the adjusted P value was < 0.01 based on the Wilcoxon rank sum test. Gene Volcano plots of DEGs were created using the R package EnhancedVolcano. Ontology analysis was performed by clusterProfiler version 4.4.4 with the org.Mm.eg.db (v3.15.0). The module scores of each gene signature were calculated using the AddModuleScore function in Seurat with default parameters. This function scores cells for the average expression levels of a set of genes, which is subtracted by the average expression of randomly selected control genes. Cellular annotation of each cluster was determined using marker genes expression and scores using previously published gene signatures [96–101] , and were used to derive the module scores for each set of cluster-defining genes using the AddModuleScore function in Seurat with default parameters. This function scores cells for the average expression levels of a set of genes, which is subtracted by the average expression of randomly selected control genes. The final annotation was manually curated and incorporated the gene signature scores but also took into account up- and down-regulated genes, and weighted key markers.

Data Analysis of Single-Cell TCR-Sequencing

Cells that possessed productive TCR α and β chains were incorporated into the analysis. We removed cells that possessed more than single α or β chain for the analysis (603 cells (9.6%) in

6 wpi samples, 2755 cells (13%) in 41 wpi samples). We defined the expanded clonal cells as a pair of TCR α and β chains that appeared in at least six cells. dittoSeq was used for bar plots [102].

Identification of TCR motifs with shared antigen specificity using GLIPH2

We used the GLIPH2 (grouping of lymphocyte interaction by paratope hotspots) webtool (http://50.255.35 .37:8080/) to cluster TCR sequences based on presumed identical antigen recognition [103]. The GLIPH2 algorithm was applied on all of 8 libraries. We only selected clusters which contained sequences from all libraries, had at least three unique CDR3s, had similar CDR3 lengths (length_score<0.05), and shared similar V_-gene frequency distributions (vb_score<0.05).

Acknowledgments

We thank the Sanderson Center for Optical Experimentation (SCOPE) core facility at UMass Chan Medical School (Worcester, MA), which provided access to the Nikon A1 confocal and the TissueGnostics TissueFAXS SL tissue cytometer. The SCOPE TissueFAXS SL was funded by a Massachusetts Life Science Center Bits to Bytes award to Drs. Christina Baer and Dorothy Schafer. The TB10.4 and 32A tetramers were obtained from the NIH Tetramer Core Facility.

Figure legends (7869 inc spaces)

Figure 1. Infected macrophages poorly activate Mtb-specific CD8 T-cells. (A) Tetramer staining of polyclonal CD8 T-cell lines specific for Mtb32A$_{309-318}$ (left) or TB10.4$_{20-28}$ (right) following two rounds of stimulation with peptide-pulsed APC. Tetramer staining of CD4 T-cells was used a negative control (inset, lower right). (B) CD8 T-cell line recognition of TGPM that were uninfected (UI), pulsed with cognate peptide (peptide), γ-irradiated Mtb (γ-Mtb) or live Mtb H37Rv infection at initial MOIs of 10 or 20 (Rv 10, Rv 20). Bar, mean±SD. The data are representative of at least two independent experiments with 1 (A) or 3 (B) technical replicates. Statistical test: one-way ANOVA, using the Dunnett test compared to uninfected macrophages. P values: *, $p<0.05$ **, $p<0.01$; ***, $p<0.001$; #, $p<0.0001$. N.D., none detected.

Figure 2. Infected macrophages cross-present antigen but fail to activate Mtb-specific CD8 T-cells. (A) RG3 CD8 T-cells recognized TB10.4 protein-coated beads presented by TGPM. (B) RF33.70, an OVA-specific MHC I restricted CD8 hybridoma, recognized OVA-coated beads presented by uninfected, γ-irradiated Mtb, or H37Rv-infected TGPM. (C and D) Top. Representative images of H37Rv.YFP infected-TGPM stained for Sec22b without (C) or with (D) latex beads. Bottom. Mander's coefficient of Sec22b colocalization with Mtb and latex beads at the indicated time-points. Each point represents an individual Mtb-infected macrophage. (E) Effects of LPS or IFN-γ treatment on XPT of OVA-bead to OT-I CD8 T-cells. (F) RG4 CD8 T-cell recognition of H37Rv-infected B6 TGPM pre-treated with LPS or LPS+IFN-γ. (G) RG3 CD8 T-cell recognition of TGPM pre-treated with IFN-γ or not, then infected with H37Rv, pulsed with TB10.4-coated beads, or pulsed with TB10.4$_{4-11}$ peptide. Bars, mean ± SD. The data are representative of three (B) or two (C - F) independent experiments, (n=2-3 replicates/condition). Statistical analysis: one-way ANOVA of $\log_{10}$ transformed data using Dunnett's multiple comparison test compared to 0.5 ug/ml TB10.4-beads (A), two-way ANOVA with Fisher's LSD

posttest (B and G), or by one-way ANOVA with Fisher's LSD test (C - F) p-values: *, $p<0.05$; **, $p<0.01$; ***, $p<0.001$; #, $p<0.0001$.

Figure 3. High MOI infection promotes cross-presentation to CD8 T-cells.

(A) Viability (left), intracellular CFU (middle), and adjusted MOI (intracellular CFU/number of viable cells) (right) of TGPM infected overnight. (B) Representative images of 24-hour (left) and 2-hour (right) H37Rv.YFP-infected HOXB8 macrophages cultured with RG4 CD8 T-cells. Inset, enlargement of indicated macrophages. (C, D) Image analysis of HOXB8 macrophages infected with H37Rv.YFP using different conditions. For each condition, 13,000-18,000 macrophages were analyzed. (C) Percent of macrophages that were infected. (D) Distribution of bacteria/macrophage for each condition evaluated. Uninfected macrophages were excluded from analysis and the bacterial number was extrapolated as described in the *Methods*. (C and D) Bar and numbers above bar represent median. (E) DM108 CD8 T-cell recognition of HOXB8 macrophages infected for 2 or 24 hours with H37Rv. (F) RG4 (right) and P25 (left) recognition of B6-matched or BALB/c-mismatched H37Rv-infected TGPM for 2-hours (low MOI) or 24-hours (high MOI). (G) Mean T-cell contacts with infected WT or MHC $I^{-/-}$ (KO) HOXB8 macrophages as a function of intracellular bacterial content. (H) Representative image that showcases highly infected macrophages with many interacting T-cells (arrows, 9 and 10 interacting T-cells), and sparsely infected macrophages with no T-cell contacts. Data representative of two (E - H) or three (A) independent experiments. Bars represent mean ± SD (n=3 replicates/condition). Statistical testing: Ordinary one-way ANOVA testing for a linear trend between column means (A); two-way ANOVA with Šidák correction for multiple comparisons (E); or two-way ANOVA with Fisher's LSD posttest (F). p values: *, $p<0.05$; **, $p<0.01$; ***, $p<0.001$; #, $p<0.0001$. (H) Each point is mean ± SEM of T cells/macrophage at each inferred MOI. Multiple unpaired t test with Welch correction were performed, with a Two-stage step-up (Benjamini, Krieger, and

Yekutieli) and a false discovery rate set to Q=1%. The values shown in the figure represent q values.

Figure 4. Cell death contributes to cross-presentation.

(A) Schematic of scavenging assay. Primary cells were infected with H37Rv.YFP overnight. Cells were washed, and secondary cells were added and cocultured for 24 hrs. (B) Representative flow plots following co-culture of differentially stained macrophages. Initial gating reveals the percentage of bystander macrophages (Viogreen^{+}) that took up Mtb (YFP^{+}) (left). The Viogreen^{+}YFP^{+} macrophages were gated to determine the percentage that acquired Deep Red dye from primary-infected macrophages (right). (C) Representative image of scavenging assay. Arrows indicate bystander macrophages that acquired Mtb and dye from primary-infected macrophages. Inset, enlargement. (D) Analysis of the bystander macrophages showing that uptake of Mtb and primary-infected macrophages are correlated. (E) Schematic of antigen transfer assay. APC are represented as wild-type (W) or MHC I$^{-/-}$ (K) HOXB8 macrophages (e.g., K/W = infected MHC I$^{-/-}$, uninfected WT added). (F) RG4 CD8 T-cell recognition of the Mtb-infected macrophages in the antigen transfer assay. (G) RG4 recognition in supernatant transfer assay. Unfiltered culture supernatants [SUP] from Mtb-infected macrophages were added to uninfected or macrophages infected using the indicated MOIs for 24-hours. T-cell activation based on IFN-γ production. Bars, mean ± SD. Data are representative of two (B - D), three (F) or four (G) independent experiments. Statistical testing: Spearman and linear regression test (D); two-way ANOVA with Dunnett's test (F); or two-way ANOVA with Šidák correction for multiple comparisons (G). p values: *, $p<0.05$; **, $p<0.01$; ***, $p<0.001$; #, $p<0.0001$.

Figure 5. Cross-presentation is ESX-1 dependent.

(A) Adjusted MOI (left) and normalized viability of HOXB8 macrophages infected overnight at the indicated MOIs with WT H37Rv or ΔRD1 Mtb at 24 hours (center) or 48 hours (right) post-infection. (B) DM108 recognition of H37Rv or ΔRD1 Mtb-infected HOXB8 macrophages. RG4 (C) and P25 (D) recognition of H37Rv or ΔRD1 Mtb-infected TGPM. (E) RG4 recognition of WT of MHC $I^{-/-}$ macrophages infected with H37Rv, ΔRD1, ΔPhoP or ΔPhoP-complemented strains of Mtb. T-cell activation measured by IFN-γ ELISA. Bars, mean ± SD (n=3 replicates/condition). Data are representative of four (A) two (B, E) or three (C, D) independent experiments. Statistical testing: two-way ANOVA with Šidák correction. p values: *, $p<0.05$; **, $p<0.01$; ***, $p<0.001$; #, $p<0.0001$.

Figure 6. Single cell RNAseq analysis of CD8 T-cells from Mtb-infected mice.

(A) UMAP visualization of integrated analysis for CD8 T-cells, 6 and 41 wpi, after clustering without TCR genes. The clusters (0-8) are colored according to CD8 T-cell subtype. See Table S1 and Figure S6, S7 for naming rationale. (B) Percentage of CD8 T-cells from 6- (top) or 41 (bottom) wpi, in each cluster that are “RENS” or “non-RENS” CD8 T-cells [subdivided into expanded (>5) or non-expanded (≤5) cells]. (C) UMAP visualization from “A” colored according to RENS or non-RENS (expanded or non-expanded) clonotypes. (D) The number of CD8 T-cells from each time point belonging to RENS or non-RENS (expanded or non-expanded) clonotypes. (E) Distribution of CDR3β sequences from “RENS” CD8 T-cells. (F) Distribution of CDR3α sequences from “RENS” CD8 T-cells. (G) IFN-γ expression, 6 or 41 wpi among RENS or non-RENS (expanded or non-expanded) CD8 T-cells. (H) DEGs from RENS-motif expressing vs. non-RENS expanded CD8 T-cells comparison at 6 wpi. (I) Effector-like signature [100] applied to the nine clusters. (J) DEGs from RENS-motif expressing vs. non-RENS expanded CD8 T-cells comparison at 41 wpi. (H, J) Red, FC>0.5 $\log_2$ and $p<0.01$; blue, FC<0.5 $\log_2$ and $p<0.01$; green, FC>0.5 $\log_2$ and $p>0.01$; black, FC<0.5 $\log_2$ and $p>0.01$. P values are corrected for

multiple comparisons. Genes of particular interest are labelled. Integrated expression data was used for A, C, I; raw expression data for figure G, H, J.

Supplemental Tables.

Table S1. All DEGs for the nine CD8 T-cell clusters (pertains to **Figures 6A, S6).** Tab 1, description of the parameters in the table. DEGs that define the nine different CD8 T-cell clusters are listed, with sequentially numbered tabs corresponding to each cluster.

Table S2. CDR3β DNA rearrangements of TB10.4-specific CD8 T-cells with "RENS" motif (pertains to **Figures 6E, S6).** A list of the different canonical sequences with the "RENS" motif in the CDR3β region. These sequences have previously been shown to be characteristic of TCRβ chains specific for the TB10.3$_{4\text{-}11}$ epitope. This table is a cumulative list of the clonotypes present at either 6 wpi or 41 wpi and represents a total of four mice. Thus, some of the CDR3β regions are encode by more than one unique Vβ/D/Jβ recombination event.

Table S3. Genes expressed by CD8 T-cells with the "RENS" motif compared to other clonally expanded CD8 T-cells (pertains to **Figures 6H, J; S6).** Tab 1, description of the parameters in the table. List of genes differentially expressed between motif-RENS and non-RENS (expanded) CD8 T-cells at 6 wpi (Tab 2) or 41 wpi (Tab 3).

Supplemental Figure Legends.

Figure S1. Macrophages present TB10.4 produced by *Listeria monocytogenes* via the cytosolic and vacuolar XPT pathways. Thioglycolate-elicited peritoneal macrophages (TGPM) infected with TB10.4-expressing *Listeria monocytogenes* (Lm.TB10) present TB10.4 to RG3, by a listerolysin (LLO) dependent pathway. LLO breaches the phagosomal membrane and allows Lm to enter the cytosol [104]. We tested whether TB10.4 produced by Lm.TB10 would be presented by the canonical MHC I pathway. In these assays, CD69 induction by RG3 indicated T-cell activation. Uninfected (UI) cells served as the negative control. Also, Lm.TB10-infected (INF) B10.BR TGPM (H-2^k), are MHC I-mismatched APC and cannot present TB10.$4_{4\text{-}11}$ to RG3 CD8 T-cells, and thus were used to distinguish noncognate activation from cognate activation seen with Lm.TB10-infected MHC I-matched APC (i.e., B10/J TGPM, H-2^b). The proteosome inhibitors epoxomicin (Epox) and lactacystin (Lac) inhibited the <u>cytosolic</u> pathway presentation of TB10.4 to CD8 T-cells. Bafilomycin (Baf) inhibits phagosomal acidification and can be used to assess dependency on the <u>vacuolar</u> pathway [105]. In these experiments, bafilomycin abrogated MHC I presentation. As LLO requires an acidic pH to function, a confounder is that bafilomycin could interfere with XPT by directly suppressing LLO activity and diminishing cytosolic access to antigen. Therefore, another possibility is that bafilomycin inhibition of both cytosolic and vacuolar XPT pathways partially inhibited presentation of TB10.4 during Lm.TB10 infection. Alternatively, these results could reflect heterogeneity within this cell population[23,106–108]. Finally, Brefeldin A (BFA) inhibits protein transport from the ER to the Golgi and as expected, abolishes MHC I presentation [26 37]. Statistical analysis by One-way ANOVA. p values: *, $p<0.05$; **, $p<0.01$; ***, $p<0.001$; #, $p<0.0001$.

Figure S2. Markers of cross-presentation co-localize with Mtb containing compartments in infected macrophages. TGPM were infected with H37Rv.YFP for two hours at an MOI of 5, followed by extensive washing to remove any extracellular bacilli. Two or twenty-four hours after

infection, the macrophages were fixed and stained with antibodies specific for proteins known to have a role in cross-presentation by APC to CD8 T-cells. Colocalization between H37Rv.YFP and MHC I, P97, Rab5, or Cathepsin was determined by confocal fluorescent microscopy and Mander's coefficients were calculated for each infected macrophage. Each data point represents an individual macrophage. Bar, mean. Statistical analysis by one-way ANOVA with Fisher's LSD test. p values: *, $p<0.05$; **, $p<0.01$; ***, $p<0.001$; #, $p<0.0001$

Figure S3. Mtb-infected BMDC and HOXB8-differentiated DCs fail to cross-present TB10.4 to CD8 T-cells in vitro under conventional culture conditions. (A) RG4 CD8 T-cell recognition of H37Rv-infected BMDC. B6 or BALB/c BMDC (H-2-matched and mismatched, respectively) were pre-activated with LPS (100 ng/ml) or not and pulsed with TB10.$4_{4\text{-}11}$ peptide or infected with H37Rv at MOIs of 5 or 20 for two hours. After 24 hours, IFN-γ was measured as an indication of CD8 T-cell activation. (B) RG4 recognition of H37Rv-infected HOXB8-derived DC. GM-CSF HOXB8 progenitor cells were cultured in either GM-CSF or Flt3 to generate DC, or in M-CSF to generate macrophages [43,91,109]. The differentiated APC were pulsed with TB10.$4_{4\text{-}11}$ peptide as a positive control or infected with H37Rv at an MOI of 5 for 2 hours. After 24 hours, IFN-γ was measured as an indication of CD8 T-cell activation. Bars, mean ± SD. Data are representative of two (A) or four (B) independent experiments, each with 3 technical replicates/condition. Statistical analysis by one-way ANOVA with Fisher's LSD test. p values: *, $p<0.05$; ***, $p<0.001$; #, $p<0.0001$. N.D., not detected. Dotted line, upper level of detection. Not all comparisons are shown for clarity. UI, uninfected; P, peptide; INF, Mtb-infected.

Figure S4. BATF3 is not required for priming of the immunodominant CD8 T cell responses to 32A or TB10.4. Batf3 is required for the development of CD8α^+ populations and optimal cross-priming of CD8 T-cells [44]. We infected Batf3$^{-/-}$ and wild-type B6 mice to compare Mtb-specific CD8 T-cell responses using specific tetramers. We found small but statistically

insignificant decrease in 32A and TB10.4 CD8 T-cell responses 2 (A) or 4-6 (B) weeks post infection. n=5 mice/group. 4- and 6-week data were pooled form two experiments. Statistical testing by multiple t-tests. p values: *, p<0.05; **, p<0.01; ***, p<0.001; #, p<0.0001. Not all comparisons are shown for clarity.

Figure S5. Excessive macrophage cell death is associated with reduced antigen presentation to CD4 and CD8 T-cells. (A) B6 TGPMs were infected overnight with H37Rv at the indicated MOIs. After washing, RG4 CD8 or P25 CD4 T-cells were added, and T-cell recognition of the infected macrophages was based on measurement of IFN-γ after 24-hours. In this experiment, P25 CD4 T-cells more sensitively recognized Mtb-infected TGPM at lower MOIs (i.e., MOI=1). However, neither the CD4 not the CD8 T-cells recognized Mtb-infected TGPM at the highest MOI (i.e., MOI=10). (B) Viability assays using Crystal Violet (left) or ATP-luciferase (right) of TGPMs 24 hours post H37Rv infection was performed using a set of macrophages infected in parallel with the macrophages used in Fig.S5A. Bars, mean±SD. Data representative of three (A) or two (b) independent experiments with 3-6 replicates/condition. Statistical analysis by one-way ANOVA, using the Dunnett test compared to uninfected macrophages. p values: *, p<0.05; **, p<0.01; ***, p<0.001; #, p<0.0001.

Figure S6. Heatmap of differentially expressed genes. Heat map of the top 10 differentially regulated genes from each cluster. The bars above the heat map are associated with the cluster (clusters 0 – 8) and match Figure 6. Based on analysis of the top DEG, each cluster has been given a name that represents the activation state of the CD8 T-cells in the cluster. A scale for the normalized relative expression is shown.

Figure S7. Clustering, TCR pairing, and additional data from the scRNASeq analysis. (A) Clustering of CD8 T cells. Previously published gene signatures [96–101] for CD8 T cells were used

to derive the module scores for each set of cluster-defining genes using the AddModuleScore function in Seurat with default parameter. Cellular annotation of each cluster was based on the signature scores. As signatures representing different cell states had similar scores for some cell clusters, the final annotation was manually curated, and considered the gene signature scores but also up- and down-regulated genes, and weighting of key markers. (B) TCRα and TCRβ pairing among CD8 T cells with the RENS-motif (i.e., TB10.4-specific). The different CDR3α sequences associated with each conserved CDR3β amino acid sequence (e.g., 'RENS'), is quantified. CDR3α sequences with the amino acid motif "CAVSxGGRALIF", where x = G, Q, W, or E, are the most abundant TCRs. There is some promiscuity of chain pairing. Gene set and pathway enrichment analysis shows that at 41 wpi, CD8 T cells with the "RENS" motif had greater enrichment of TCR signaling and TCR-independent activation signatures, compared to other clonally expanded CD8 T cells (C), and gene ontology corresponding to cell signaling and cell-cell interactions were also enriched in "RENS" CD8 T-cells compared to other expanded CD8 T-cells (D).

References

1. World Health Organization. *Global tuberculosis report 2021*. (2021).
2. Mangtani, P. *et al.* Protection by BCG Vaccine Against Tuberculosis: A Systematic Review of Randomized Controlled Trials. *Clinical Infectious Diseases* **58**, 470–480 (2014).
3. Luca, S. & Mihaescu, T. History of BCG Vaccine. *Maedica* **8**, 53–8 (2013).
4. North, R. J. & Jung, Y.-J. Immunity to Tuberculosis. *Annual Review of Immunology* **22**, 599–623 (2004).
5. Furin, J., Cox, H. & Pai, M. Tuberculosis. *The Lancet* **393**, 1642–1656 (2019).
6. O'Garra, A. *et al. The Immune Response in Tuberculosis*. *Annual Review of Immunology* vol. 31 (2013).
7. Orme, I. M. & Collins, F. M. Protection against Mycobacterium tuberculosis infection by adoptive immunotherapy. Requirement for T cell-deficient recipients. *Journal of Experimental Medicine* **158**, 74–83 (1983).
8. Leveton, C. *et al.* T-cell-mediated protection of mice against virulent Mycobacterium tuberculosis. *Infection and Immunity* **57**, 390–395 (1989).
9. Mogues, T., Goodrich, M. E., Ryan, L., LaCourse, R. & North, R. J. The relative importance of T cell subsets in immunity and immunopathology of airborne Mycobacterium tuberculosis infection in mice. *J Exp Med* **193**, 271–80 (2001).
10. Lu, Y. J. *et al.* CD4 T cell help prevents CD8 T cell exhaustion and promotes control of Mycobacterium tuberculosis infection. *Cell Reports* **36**, (2021).
11. Ernst, J. D. Mechanisms of M. tuberculosis Immune Evasion as Challenges to TB Vaccine Design. *Cell Host & Microbe* **24**, 34–42 (2018).
12. Behar, S. M., Carpenter, S. M., Booty, M. G., Barber, D. L. & Jayaraman, P. Orchestration of pulmonary t cell immunity during mycobacterium tuberculosis infection: Immunity interruptus. *Seminars in Immunology* **26**, 559–577 (2014).
13. Khan, S. H. & Badovinac, V. P. Listeria monocytogenes: a model pathogen to study antigen-specific memory CD8 T cell responses. *Semin Immunopathol* **37**, 301 (2015).
14. Schmidt, M. E. & Varga, S. M. The CD8 T cell response to respiratory virus infections. *Frontiers in Immunology* **9**, 678 (2018).
15. Rock, K. L., Reits, E. & Neefjes, J. Present Yourself! By MHC Class I and MHC Class II Molecules. *Trends in Immunology* vol. 37 724–737 Preprint at https://doi.org/10.1016/j.it.2016.08.010 (2016).
16. Blander, J. M. Regulation of the Cell Biology of Antigen Cross-Presentation. *Annual Review of Immunology* **36**, 717–753 (2018).

17. Cruz, F. M., Colbert, J. D., Merino, E., Kriegsman, B. A. & Rock, K. L. The Biology and Underlying Mechanisms of Cross-Presentation of Exogenous Antigens on MHC-I Molecules. *Annu Rev Immunol* (2017) doi:10.1146/annurev-immunol-041015-055254.

18. Fonteneau, J. F. *et al.* Characterization of the MHC class I cross-presentation pathway for cell-associated antigens by human dendritic cells. *Blood* **102**, 4448–4455 (2003).

19. Burgdorf, S., Schölz, C., Kautz, A., Tampé, R. & Kurts, C. Spatial and mechanistic separation of cross-presentation and endogenous antigen presentation. *Nat Immunol* **9**, 558–66 (2008).

20. Saveanu, L. *et al.* Class I Cross-Presentation. **325**, 213–218 (2009).

21. Tiwari, N. *et al.* A transporter associated with antigen-processing independent vacuolar pathway for the MHC class I-mediated presentation of endogenous transmembrane proteins. *J Immunol* **178**, 7932–7942 (2007).

22. Cruz-Leal, Y. *et al.* The Vacuolar Pathway in Macrophages Plays a Major Role in Antigen Cross-Presentation Induced by the Pore-Forming Protein Sticholysin II Encapsulated Into Liposomes. *Front Immunol* **9**, 2473 (2018).

23. Muntjewerff, E., Meesters, L. & van den Bogaart, G. Antigen Cross-Presentation by Macrophages. *Frontiers in Immunology* **11**, 1276 (2020).

24. Lee, J. *et al.* CD11cHi monocyte-derived macrophages are a major cellular compartment infected by Mycobacterium tuberculosis. *PLOS Pathogens* **16**, e1008621 (2020).

25. Woodworth, J. S. *et al.* Mycobacterium tuberculosis directs immunofocusing of CD8+ T cell responses despite vaccination. *J Immunol* **186**, 1627–37 (2011).

26. Carpenter, S. M., Nunes-Alves, C., Booty, M. G., Way, S. S. & Behar, S. M. A Higher Activation Threshold of Memory CD8+ T Cells Has a Fitness Cost That Is Modified by TCR Affinity during Tuberculosis. *PLoS Pathogens* **12**, (2016).

27. Nunes-Alves, C. *et al.* Human and Murine Clonal CD8+ T Cell Expansions Arise during Tuberculosis Because of TCR Selection. *PLoS Pathogens* **11**, 1–29 (2015).

28. Sutiwisesak, R. *et al.* A natural polymorphism of Mycobacterium tuberculosis in the esxH gene disrupts immunodomination by the TB10.4-specific CD8 T cell response. *PLOS Pathogens* **16**, e1009000 (2020).

29. Yang, J. D. *et al.* Mycobacterium tuberculosis-specific CD4+ and CD8+ T cells differ in their capacity to recognize infected macrophages. *PLOS Pathogens* **14**, e1007060 (2018).

30. Brandt, L. *et al.* The protective effect of the Mycobacterium bovis BCG vaccine is increased by coadministration with the Mycobacterium tuberculosis 72-kilodalton fusion polyprotein Mtb72F in M. tuberculosis-infected guinea pigs. *Infection and Immunity* **72**, 6622–6632 (2004).

31. Ahn, S. S. *et al.* Mtb32 is a promising tuberculosis antigen for DNA vaccination in pre-and post-exposure mouse models. *Gene Therapy* **19**, 570–575 (2012).

32. Mazzaccaro, R. J. *et al.* Major histocompatibility class I presentation of soluble antigen facilitated by Mycobacterium tuberculosis infection. *Immunology Contributed by Barry R. Bloom* **93**, 11786–11791 (1996).

33. Alloatti, A. *et al.* Critical role for Sec22b-dependent antigen cross- presentation in antitumor immunity. *Journal of Experimental Medicine* 1–11 (2017) doi:10.1084/jem.20170229.

34. Cebrian, I. *et al.* Sec22b regulates phagosomal maturation and antigen crosspresentation by dendritic cells. *Cell* **147**, 1355–1368 (2011).

35. Wu, S. J. *et al.* A Critical Analysis of the Role of SNARE Protein SEC22B in Antigen Cross-Presentation. *Cell Reports* **19**, 2645–2656 (2017).

36. Ménager, J. *et al.* Cross-Presentation of Synthetic Long Peptides by Human Dendritic Cells: A Process Dependent on ERAD Component p97/VCP but Not sec61 and/or Derlin-1. *PLoS ONE* **9**, e89897 (2014).

37. Anderson, D. J. *et al.* Targeting the AAA ATPase p97 as an Approach to Treat Cancer through Disruption of Protein Homeostasis. *Cancer Cell* **28**, 653–665 (2015).

38. Arnold, C. E., Gordon, P., Barker, R. N. & Wilson, H. M. The activation status of human macrophages presenting antigen determines the efficiency of Th17 responses. *Immunobiology* **220**, 10–19 (2015).

39. Celhar, T. *et al.* TLR7 and TLR9 ligands regulate antigen presentation by macrophages. *International Immunology* **28**, 223–232 (2016).

40. Sánchez, D. *et al.* Role of TLR2- and TLR4-mediated signaling in Mycobacterium tuberculosis-induced macrophage death. *Cellular Immunology* **260**, 128–136 (2010).

41. Carmona, J. *et al.* Mycobacterium tuberculosis Strains Are Differentially Recognized by TLRs with an Impact on the Immune Response. *PLoS ONE* **8**, e67277 (2013).

42. Wang, G. G. *et al.* Quantitative production of macrophages or neutrophils ex vivo using conditional Hoxb8. *Nature Methods* **3**, 287–293 (2006).

43. Mayer, C. T. *et al.* Selective and efficient generation of functional Batf3-dependent CD1031 dendritic cells from mouse bone marrow. *Blood* **124**, 3081–3091 (2014).

44. Hildner, K. *et al.* Batf3 deficiency reveals a critical role for CD8α+ dendritic cells in cytotoxic T cell immunity. *Science (1979)* **322**, 1097–1100 (2008).

45. Tussiwand, R. *et al.* Compensatory dendritic cell development mediated by BATF-IRF interactions. *Nature* **490**, 502–7 (2012).

46. Patankar, Y. R. *et al.* Limited recognition of Mycobacterium tuberculosis-infected macrophages by polyclonal CD4 and CD8 T cells from the lungs of infected mice. *Mucosal Immunology* **13**, 140 (2020).

47. Rothchild, A. C. *et al.* Role of Granulocyte-Macrophage Colony-Stimulating Factor Production by T Cells during *Mycobacterium tuberculosis* Infection. *mBio* **8**, (2017).

48. Rothchild, A. C. *et al.* iNKT Cell Production of GM-CSF Controls Mycobacterium tuberculosis. *PLoS Pathogens* **10**, e1003805 (2014).

49. Mittal, E. *et al.* Mycobacterium tuberculosis Type VII Secretion System Effectors Differentially Impact the ESCRT Endomembrane Damage Response. *mBio* **9**, e01765-18 (2018).

50. Portal-Celhay, C. *et al.* Mycobacterium tuberculosis EsxH inhibits ESCRT-dependent CD4(+) T-cell activation. *Nat Microbiol* **2**, 16232 (2016).

51. Behar, S. M., Martin, C. J., Nunes-Alves, C., Divangahi, M. & Remold, H. G. Lipids, apoptosis, and cross-presentation: links in the chain of host defense against Mycobacterium tuberculosis. *Microbes and Infection* **13**, 749–756 (2011).

52. Divangahi, M., Desjardins, D., Nunes-Alves, C., Remold, H. G. & Behar, S. M. Eicosanoid pathways regulate adaptive immunity to Mycobacterium tuberculosis. *Nature Immunology* **11 VN-r**, 751–758 (2010).

53. Martin, C. J. *et al.* Efferocytosis is an innate antibacterial mechanism. *Cell Host and Microbe* **12**, 289–300 (2012).

54. Chen, M. *et al.* Lipid mediators in innate immunity against tuberculosis: opposing roles of PGE2 and LXA4 in the induction of macrophage death. *J Exp Med* **205**, 2791–801 (2008).

55. Lee, J., Remold, H. G., Ieong, M. H. & Kornfeld, H. Macrophage Apoptosis in Response to High Intracellular Burden of Mycobacterium tuberculosis Is Mediated by a Novel Caspase-Independent Pathway. *The Journal of Immunology* **176**, 4267–4274 (2006).

56. Lee, J., Repasy, T., Papavinasasundaram, K., Sassetti, C. & Kornfeld, H. Mycobacterium tuberculosis Induces an Atypical Cell Death Mode to Escape from Infected Macrophages. *PLoS ONE* **6**, e18367 (2011).

57. Repasy, T. *et al.* Intracellular Bacillary Burden Reflects a Burst Size for Mycobacterium tuberculosis In Vivo. *PLoS Pathogens* **9**, e1003190 (2013).

58. Mahamed, D. *et al.* Intracellular growth of Mycobacterium tuberculosis after macrophage cell death leads to serial killing of host cells. *Elife* **6**, (2017).

59. Dallenga, T. *et al.* M. tuberculosis-Induced Necrosis of Infected Neutrophils Promotes Bacterial Growth Following Phagocytosis by Macrophages. *Cell Host and Microbe* **22**, 519-530.e3 (2017).

60. Martin, C. J., Peters, K. N. & Behar, S. M. Macrophages clean up: efferocytosis and microbial control. *Current Opinion in Microbiology* **17**, 17–23 (2014).

61. Hsu, T. *et al.* The primary mechanism of attenuation of bacillus Calmette-Guérin is a loss of secreted lytic function required for invasion of lung interstitial tissue. *Proc Natl Acad Sci U S A* **100**, 12420–12425 (2003).

62. Abdallah, A. M. *et al.* Type VII secretion--mycobacteria show the way. *Nat Rev Microbiol* **5**, 883–891 (2007).

63. Hsu, T. *et al.* The primary mechanism of attenuation of bacillus Calmette-Guerin is a loss of secreted lytic function required for invasion of lung interstitial tissue. *Proc Natl Acad Sci U S A* **100**, 12420–5 (2003).

64. Ryndak, M., Wang, S. & Smith, I. PhoP, a key player in Mycobacterium tuberculosis virulence. *Trends in Microbiology* **16**, 528–534 (2008).

65. Gonzalo-Asensio, J. *et al.* PhoP: A missing piece in the intricate puzzle of Mycobacterium tuberculosis virulence. *PLoS ONE* **3**, e3496 (2008).

66. Cimino, M. *et al.* Identification of DNA binding motifs of the mycobacterium tuberculosis phop/phor two-component signal transduction system. *PLoS ONE* **7**, e42876 (2012).

67. Akter, S. *et al.* Mycobacterium tuberculosis infection drives a type I IFN signature in lung lymphocytes. *Cell Reports* **39**, (2022).

68. Quigley, M. F. *et al.* Convergent recombination shapes the clonotypic landscape of the naïve T-cell repertoire. *Proc Natl Acad Sci U S A* **107**, 19414–19419 (2010).

69. Venturi, V. *et al.* Sharing of T cell receptors in antigen-specific responses is driven by convergent recombination. *Proc Natl Acad Sci U S A* **103**, 18691–18696 (2006).

70. Lewinsohn, D. A. *et al.* Mycobacterium tuberculosis-specific CD8+ T Cells Preferentially Recognize Heavily Infected Cells. *American Journal of Respiratory and Critical Care Medicine* **168**, 1346–1352 (2003).

71. Hoffmann, P. R. *et al.* Phosphatidylserine (PS) induces PS receptor–mediated macropinocytosis and promotes clearance of apoptotic cells. *The Journal of Cell Biology* **155**, 649 (2001).

72. Yin, C. & Heit, B. Cellular Responses to the Efferocytosis of Apoptotic Cells. *Front Immunol* **12**, 631714 (2021).

73. Desch, A. N. *et al.* CD103+ pulmonary dendritic cells preferentially acquire and present apoptotic cell–associated antigen. *Journal of Experimental Medicine* **208**, 1789–1797 (2011).

74. Tzelepis, F. *et al.* Annexin1 regulates DC efferocytosis and cross-presentation during Mycobacterium tuberculosis infection. *Journal of Clinical Investigation* **125**, 752–768 (2015).

75. Canton, J. *et al.* The receptor DNGR-1 signals for phagosomal rupture to promote cross-presentation of dead-cell-associated antigens. *Nature Immunology* **22**, 140–153 (2021).

76. Zelenay, S. *et al.* The dendritic cell receptor DNGR-1 controls endocytic handling of necrotic cell antigens to favor cross-priming of CTLs in virus-infected mice. *Journal of Clinical Investigation* **122**, 1615–1627 (2012).

77. Schulz, O. *et al.* Myosin II Synergizes with F-Actin to Promote DNGR-1-Dependent Cross-Presentation of Dead Cell-Associated Antigens. *Cell Reports* vol. 24 419–428 (2018).

78. van der Wel, N. *et al.* M. tuberculosis and M. leprae translocate from the phagolysosome to the cytosol in myeloid cells. *Cell* **129**, 1287–98 (2007).

79. Manzanillo, P. S., Shiloh, M. U., Portnoy, D. A. & Cox, J. S. Mycobacterium tuberculosis activates the DNA-dependent cytosolic surveillance pathway within macrophages. *Cell Host and Microbe* **11**, 469–480 (2012).

80. Divangahi, M., Behar, S. M. & Remold, H. Dying to live: how the death modality of the infected macrophage affects immunity to tuberculosis. *Adv Exp Med Biol* **783**, 103 (2013).

81. Larson, S. R. *et al.* Ly6C+ monocyte efferocytosis and cross-presentation of cell-associated antigens. *Cell Death & Differentiation* **23**, 997–1003 (2016).

82. Balam, S. *et al.* Cross-presentation of dead-cell-associated antigens by DNGR-1+ dendritic cells contributes to chronic allograft rejection in mice. *European Journal of Immunology* **00**, 1–14 (2020).

83. Woodworth, J. S., Fortune, S. M. & Behar, S. M. Bacterial Protein Secretion Is Required for Priming of CD8+ T Cells Specific for the Mycobacterium tuberculosis Antigen CFP10. *Infection and Immunity* **76**, 4199–4205 (2008).

84. Maurice, N. J., Taber, A. K. & Prlic, M. The Ugly Duckling Turned to Swan: A Change in Perception of Bystander-Activated Memory CD8 T Cells. *The Journal of Immunology* **206**, 455–462 (2021).

85. Bangs, S. C. *et al.* Human CD4+ memory T cells are preferential targets for bystander activation and apoptosis. *J Immunol* **182**, 1962–71 (2009).

86. Leruste, A. *et al.* Clonally Expanded T Cells Reveal Immunogenicity of Rhabdoid Tumors. *Cancer Cell* **36**, 597-612.e8 (2019).

87. Sandu, I. *et al.* Landscape of Exhausted Virus-Specific CD8 T Cells in Chronic LCMV Infection. *Cell Rep* **32**, 108078 (2020).

88. Chihara, N. *et al.* Induction and transcriptional regulation of the co-inhibitory gene module in T cells. *Nature* **558**, 454–459 (2018).

89. Grant, N. L. *et al.* T cell transcription factor expression evolves over time in granulomas from Mycobacterium tuberculosis-infected cynomolgus macaques. *Cell Reports* **39**, 110826 (2022).

90. Gideon, H. P. *et al.* Multimodal profiling of lung granulomas reveals cellular correlates of tuberculosis control. *bioRxiv* 2020.10.24.352492 (2021) doi:10.1101/2020.10.24.352492.

91. Wang, G. G. *et al.* Quantitative production of macrophages or neutrophils ex vivo using conditional Hoxb8. *Nat Methods* **3**, 287–93 (2006).

92. Helft, J., Bö, J., Schraml, B. U. & Goubau, D. GM-CSF Mouse Bone Marrow Cultures Comprise a Heterogeneous Population of CD11c + MHCII + Macrophages and Dendritic Cells. *Immunity* **42**, 1197–1211 (2015).

93. Barrios, K. & Celis, E. TriVax-HPV: an improved peptide-based therapeutic vaccination strategy against human papillomavirus-induced cancers. *Cancer Immunology, Immunotherapy* **61**, 1307–1317 (2012).

94. Stuart, T. *et al.* Comprehensive Integration of Single-Cell Data. *Cell* **177**, 1888-1902.e21 (2019).

95. McGinnis, C. S., Murrow, L. M. & Gartner, Z. J. DoubletFinder: Doublet Detection in Single-Cell RNA Sequencing Data Using Artificial Nearest Neighbors. *Cell Systems* **8**, 329-337.e4 (2019).

96. Cassetta, L. *et al.* Human Tumor-Associated Macrophage and Monocyte Transcriptional Landscapes Reveal Cancer-Specific Reprogramming, Biomarkers, and Therapeutic Targets. *Cancer Cell* **35**, 588-602.e10 (2019).

97. Clarke, J. *et al.* Single-cell transcriptomic analysis of tissue-resident memory T cells in human lung cancer. *J Exp Med* **216**, 2128–2149 (2019).

98. Pace, L. *et al.* The epigenetic control of stemness in CD8+ T cell fate commitment. *Science* **359**, 177–186 (2018).

99. Szabo, P. A. *et al.* Single-cell transcriptomics of human T cells reveals tissue and activation signatures in health and disease. *Nat Commun* **10**, 4706 (2019).

100. Miller, B. C. *et al.* Subsets of exhausted CD8+ T cells differentially mediate tumor control and respond to checkpoint blockade. *Nat Immunol* **20**, 326–336 (2019).

101. Utzschneider, D. T. *et al.* T Cell Factor 1-Expressing Memory-like CD8(+) T Cells Sustain the Immune Response to Chronic Viral Infections. *Immunity* **45**, 415–27 (2016).

102. Bunis, D. G., Andrews, J., Fragiadakis, G. K., Burt, T. D. & Sirota, M. DittoSeq: Universal user-friendly single-cell and bulk RNA sequencing visualization toolkit. *Bioinformatics* **36**, 5535–5536 (2020).

103. Huang, H. *et al.* Analyzing the M. tuberculosis immune response by T cell receptor clustering with GLIPH2 and genome-wide antigen screening HHS Public Access Author manuscript. *Nat Biotechnol* **38**, 1194–1202 (2020).

104. Beauregard, K. E., Lee , K.-D., Collier, R. J. & Swanson, J. A. pH-dependent Perforation of Macrophage Phagosomes by Listeriolysin O from Listeria monocytogenes. *Journal of Experimental Medicine* **186**, 1159–1163 (1997).

105. Possamaï, D. *et al.* MHC class I antigen cross-presentation mediated by PapMV nanoparticles in human antigen-presenting cells is dependent on autophagy. *PLOS ONE* **16**, e0261987 (2021).

106. Pfeifer, J. D. *et al.* Phagocytic processing of bacterial antigens for class I MHC presentation to T cells. *Nature* **361**, 359–362 (1993).

107. Ruedl, C., Storni, T., Lechner, F., Bächi, T. & Bachmann, M. F. Cross-presentation of virus-like particles by skin-derived CD8– dendritic cells: a dispensable role for TAP. *European Journal of Immunology* **32**, 818 (2002).

108. Goubau, D. *et al.* Transcriptional re-programming of primary macrophages reveals distinct apoptotic and anti-tumoral functions of IRF-3 and IRF-7. *European Journal of Immunology* **39**, 527–540 (2009).

109. Rosas, M. *et al.* Hoxb8 conditionally immortalised macrophage lines model inflammatory monocytic cells with important similarity to dendritic cells. *European Journal of Immunology* **41**, 356–365 (2011).

Fig.1

A

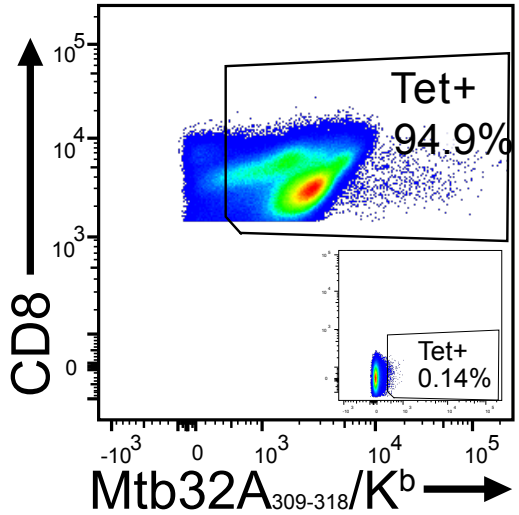
Tet+
94.9%
Tet+
0.14%
CD8
Mtb32A309-318/Kb

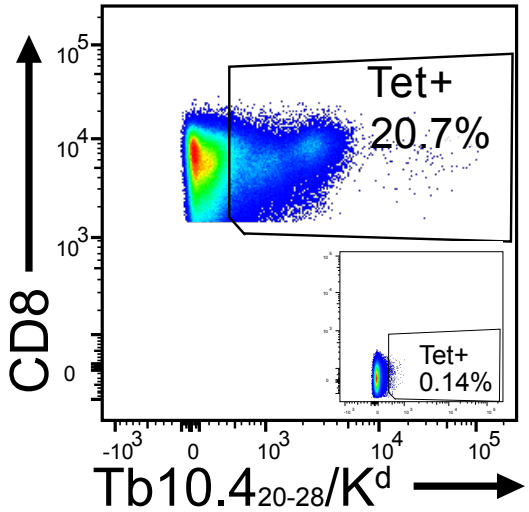
Tet+
20.7%
Tet+
0.14%
CD8
Tb10.420-28/Kd

B

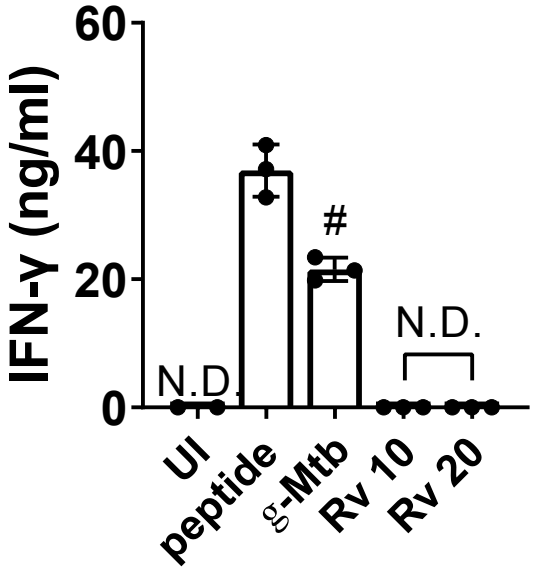
IFN-γ (ng/ml)
N.D.
#
N.D.
UI
peptide
g-Mtb
Rv 10
Rv 20

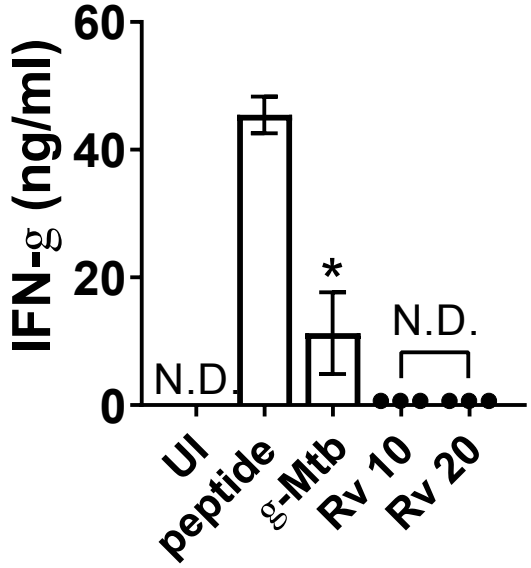
IFN-g (ng/ml)
N.D.
*
N.D.
UI
peptide
g-Mtb
Rv 10
Rv 20

Fig. 2

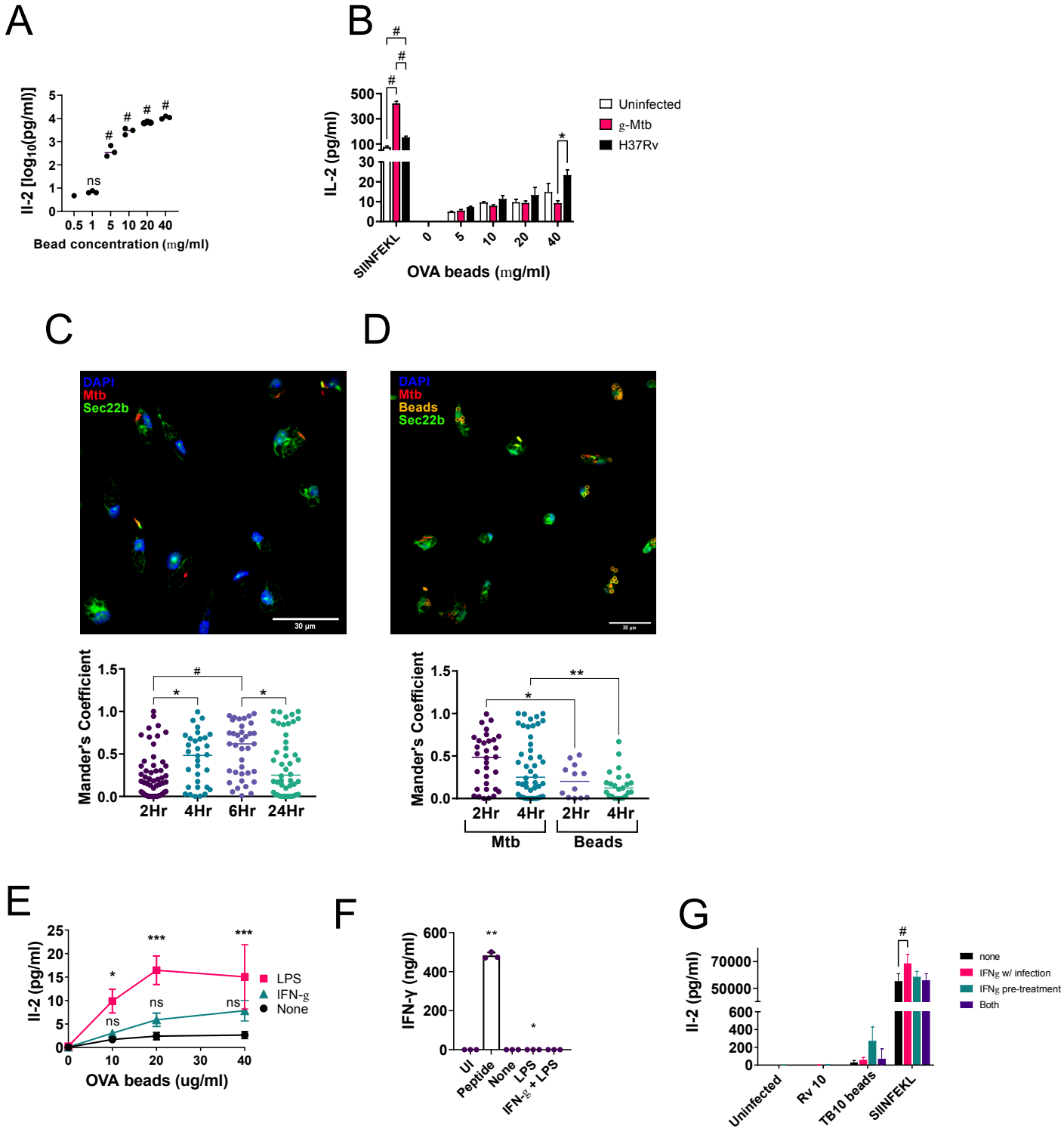
A
Il-2 [log10(pg/ml)]
Bead concentration (mg/ml)
ns
B
IL-2 (pg/ml)
OVA beads (mg/ml)
SIINFEKL
Uninfected
g-Mtb
H37Rv
C
DAPI
Mtb
Sec22b
30 µm
Mander's Coefficient
2Hr
4Hr
6Hr
24Hr
D
DAPI
Mtb
Beads
Sec22b
Mander's Coefficient
2Hr
4Hr
2Hr
4Hr
Mtb
Beads
E
Il-2 (pg/ml)
OVA beads (ug/ml)
LPS
IFN-g
None
ns
F
IFN-γ (ng/ml)
UI
Peptide
None
LPS
IFN-g + LPS
G
Il-2 (pg/ml)
Uninfected
Rv 10
TB10 beads
SIINFEKL
none
IFNg w/ infection
IFNg pre-treatment
Both

Fig. 3

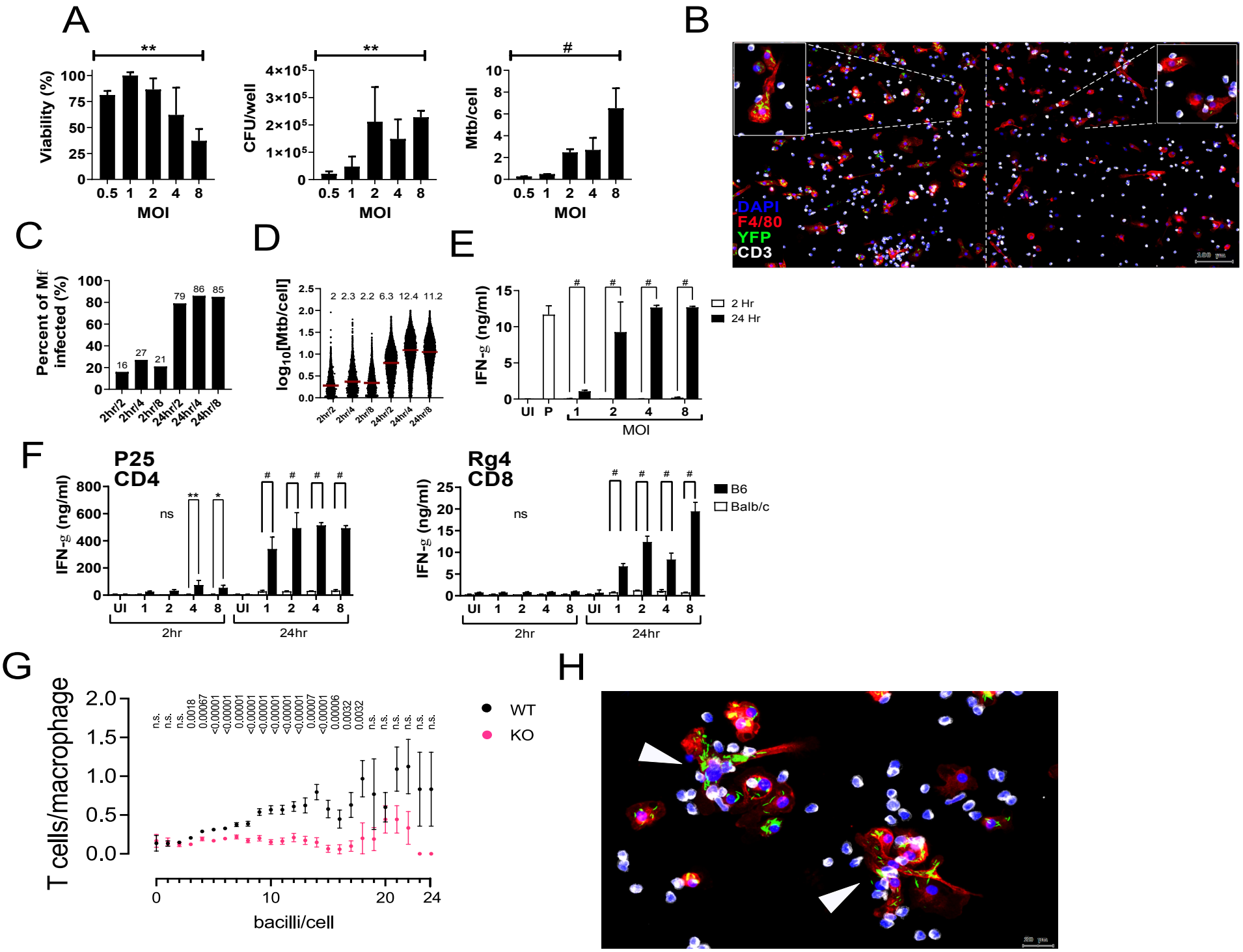
A
Viability (%)
MOI
CFU/well
Mtb/cell
B
DAPI
F4/80
YFP
CD3
C
Percent of Mf infected (%)
D
log10[Mtb/cell]
E
IFN-g (ng/ml)
2 Hr
24 Hr
UI
P
MOI
F
P25
CD4
Rg4
CD8
ns
2hr
24hr
B6
Balb/c
G
T cells/macrophage
bacilli/cell
WT
KO
H

Fig. 4

A

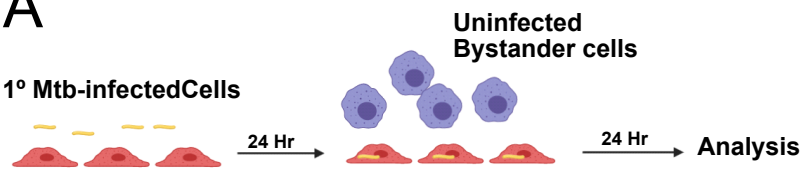

B

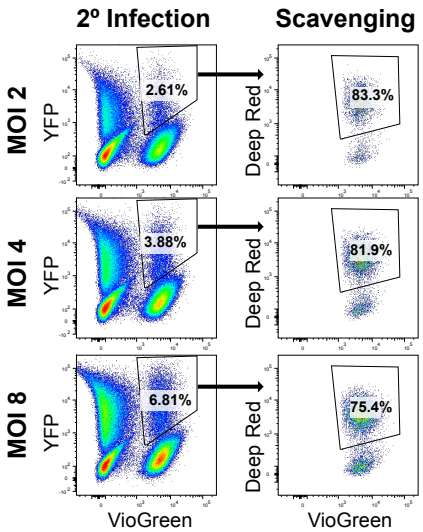

C

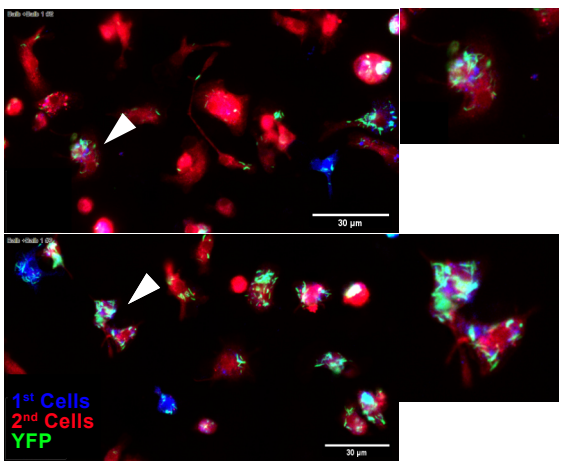

D

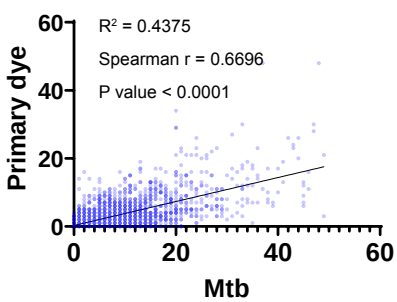

E

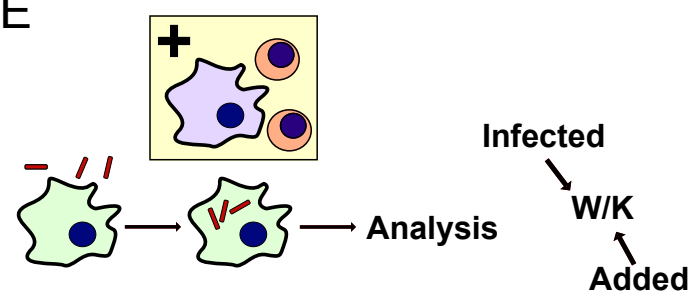

F

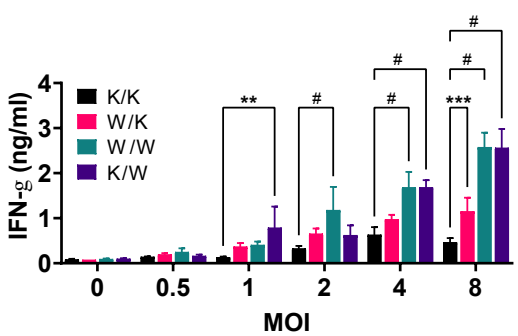

G

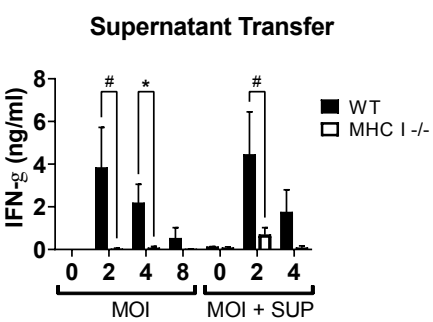

Fig. 5

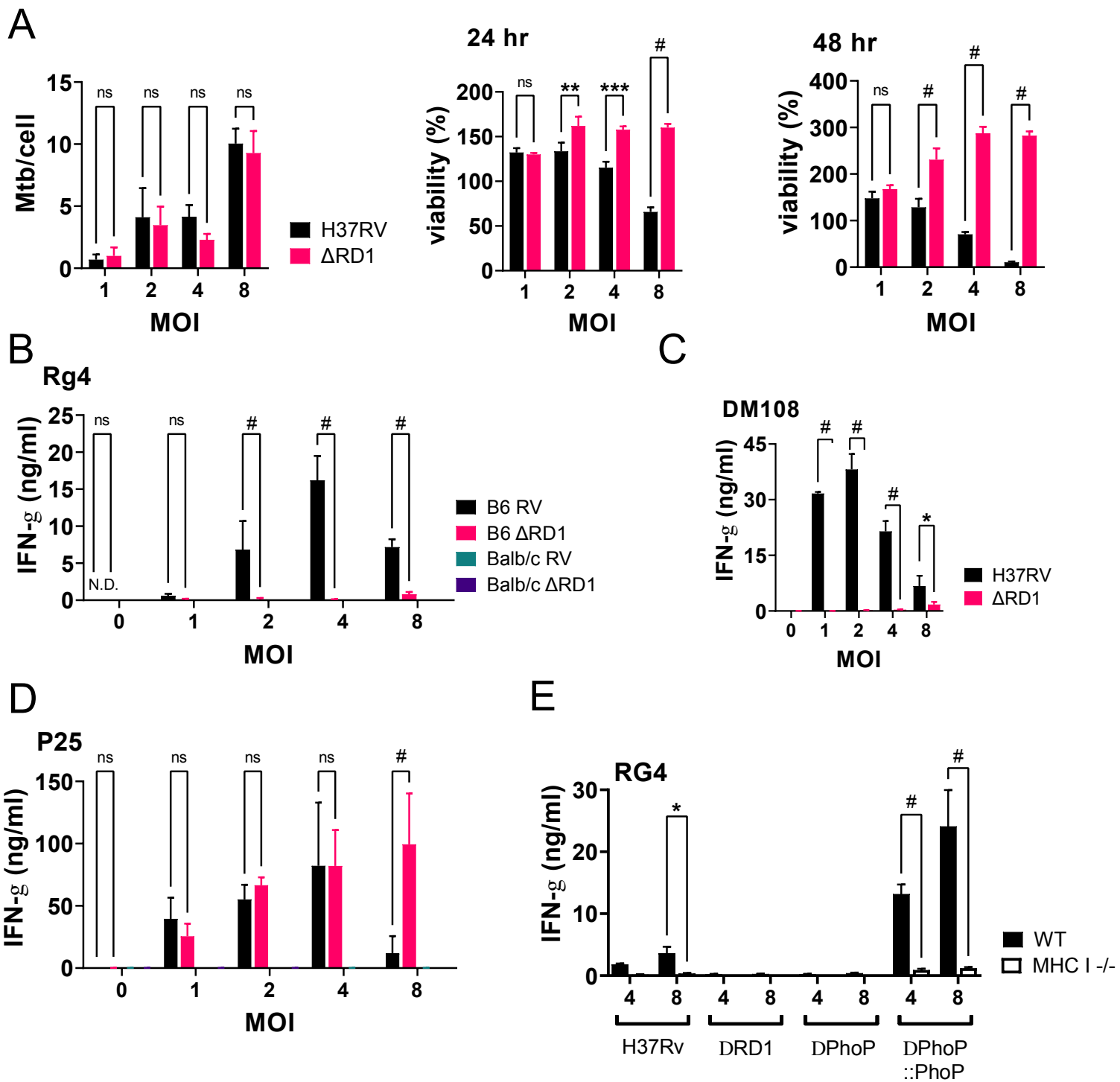
A
Mtb/cell
15
10
5
0
ns
ns
ns
ns
1
2
4
8
MOI
H37RV
ΔRD1
24 hr
viability (%)
200
150
100
50
0
ns
**
***
#
1
2
4
8
MOI
48 hr
viability (%)
400
300
200
100
0
ns
#
#
#
1
2
4
8
MOI
B
Rg4
IFN-g (ng/ml)
25
20
15
10
5
0
ns
ns
#
#
#
N.D.
0
1
2
4
8
MOI
B6 RV
B6 ΔRD1
Balb/c RV
Balb/c ΔRD1
C
DM108
IFN-g (ng/ml)
45
30
15
0
#
#
#
*
0
1
2
4
8
MOI
H37RV
ΔRD1
D
P25
IFN-g (ng/ml)
150
100
50
0
ns
ns
ns
ns
#
0
1
2
4
8
MOI
E
RG4
IFN-g (ng/ml)
30
20
10
0
*
#
#
4
8
4
8
4
8
4
8
H37Rv
DRD1
DPhoP
DPhoP
::PhoP
WT
MHC I -/-

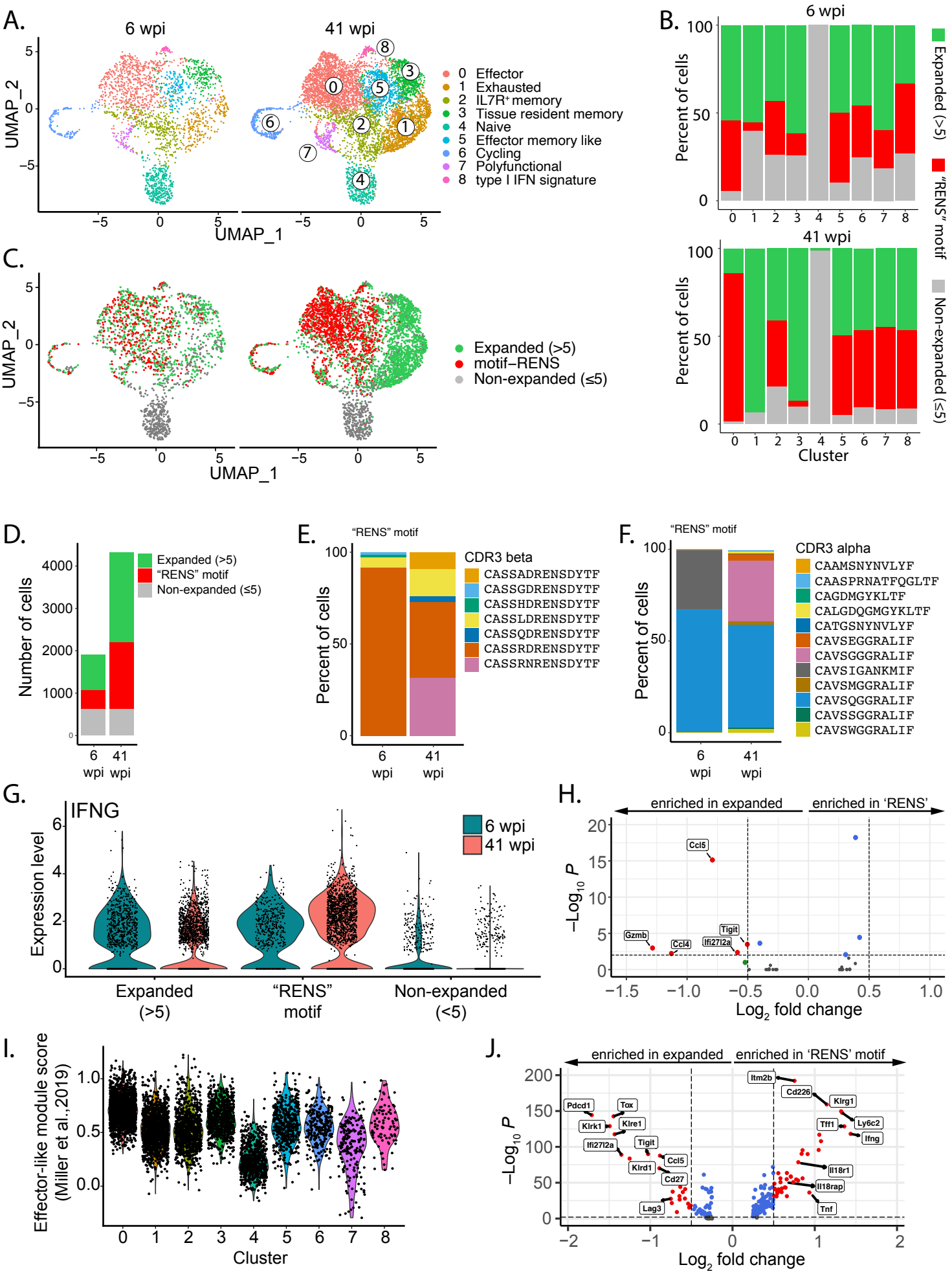
A.
6 wpi
41 wpi
UMAP_2
UMAP_1
0 Effector
1 Exhausted
2 IL7R+ memory
3 Tissue resident memory
4 Naive
5 Effector memory like
6 Cycling
7 Polyfunctional
8 type I IFN signature
B.
6 wpi
41 wpi
Percent of cells
Cluster
Expanded (>5)
"RENS" motif
Non-expanded (≤5)
C.
Expanded (>5)
motif–RENS
Non-expanded (≤5)
D.
Number of cells
Expanded (>5)
"RENS" motif
Non-expanded (≤5)
6 wpi
41 wpi
E.
"RENS" motif
Percent of cells
CDR3 beta
CASSADRENSDYTF
CASSGDRENSDYTF
CASSHDRENSDYTF
CASSLDRENSDYTF
CASSQDRENSDYTF
CASSRDRENSDYTF
CASSRNRENSDYTF
F.
"RENS" motif
Percent of cells
CDR3 alpha
CAAMSNYNVLYF
CAASPRNATFQGLTF
CAGDMGYKLTF
CALGDQGMGYKLTF
CATGSNYNVLYF
CAVSEGGRALIF
CAVSGGGRALIF
CAVSIGANKMIF
CAVSMGGRALIF
CAVSQGGRALIF
CAVSSGGRALIF
CAVSWGGRALIF
G.
IFNG
Expression level
6 wpi
41 wpi
Expanded (>5)
"RENS" motif
Non-expanded (<5)
H.
enriched in expanded
enriched in 'RENS'
−Log10 P
Log2 fold change
Ccl5
Gzmb
Ccl4
Tigit
Ifi27l2a
I.
Effector-like module score (Miller et al.,2019)
Cluster
J.
enriched in expanded
enriched in 'RENS' motif
−Log10 P
Log2 fold change
Itm2b
Cd226
Klrg1
Pdcd1
Tox
Klrk1
Klre1
Tff1
Ly6c2
Ifng
Ifi27l2a
Tigit
Ccl5
Klrd1
Cd27
Il18r1
Il18rap
Lag3
Tnf

Figure 6